nature immunology

Kinases Mst1 and Mst2 positively regulate phagocytic induction of reactive oxygen species and bactericidal activity

Jing Geng[1,8], Xiufeng Sun[1,8], Ping Wang[1], Shihao Zhang[1], Xiaozhen Wang[1], Hongtan Wu[1], Lixin Hong[1], Changchuan Xie[1], Xun Li[2], Hao Zhao[1], Qingxu Liu[1], Mingting Jiang[1], Qinghua Chen[1], Jinjia Zhang[1], Yang Li[1], Siyang Song[1], Hong-Rui Wang[1], Rongbin Zhou[3], Randy L Johnson[4], Kun-Yi Chien[5], Sheng-Cai Lin[1], Jiahuai Han[1], Joseph Avruch[6,7], Lanfen Chen[1] & Dawang Zhou[1]

Mitochondria need to be juxtaposed to phagosomes for the synergistic production of ample reactive oxygen species (ROS) in phagocytes to kill pathogens. However, how phagosomes transmit signals to recruit mitochondria has remained unclear. Here we found that the kinases Mst1 and Mst2 functioned to control ROS production by regulating mitochondrial trafficking and mitochondrion-phagosome juxtaposition. Mst1 and Mst2 activated the GTPase Rac to promote Toll-like receptor (TLR)-triggered assembly of the TRAF6-ECSIT complex that is required for the recruitment of mitochondria to phagosomes. Inactive forms of Rac, including the human Rac2^{D57N} mutant, disrupted the TRAF6-ECSIT complex by sequestering TRAF6 and substantially diminished ROS production and enhanced susceptibility to bacterial infection. Our findings demonstrate that the TLR-Mst1-Mst2-Rac signaling axis is critical for effective phagosome-mitochondrion function and bactericidal activity.

Phagocytes are specialized cells of the immune system that engulf harmful microorganisms and destroy them in phagosomes[1,2]. The destruction process depends mainly on the production of large amounts of reactive oxygen species (ROS), long thought to be generated entirely via the NADPH oxidase machinery at the phagosomal membrane[3,4]. The 'GTP-charged' active form of the Rho-family GTPases Rac1 and Rac2 is required for phagosomal activation of NADPH oxidase[5]. In unstimulated phagocytes, GDP-charged inactive Rac1 and Rac2 form a complex with a Rho-GDP–dissociation inhibitor. The activation of Rac1 and Rac2 is initiated by their release from that inhibitor, which results in part from phosphorylation of the inhibitor by the kinase PAK or PKC-α[6,7]. The importance of Rac-GTP in phagocyte function is illustrated by a human immunodeficiency syndrome characterized by severe bacterial infections that arise from a mutation in the gene encoding Rac2 that generates the D57N substitution of Rac2 (Rac2^{D57N}), which results in constitutive binding of GDP, accompanied by impaired ROS production, in phagocytes[8–10].

In addition to phagosomal activity of NADPH oxidase, maximal phagocytic generation of ROS and bactericidal activity require the production of mitochondrial ROS (mROS)[11–15]. The engagement of a subset of macrophage Toll-like receptors (TLR1, TLR2 and TLR4) leads to the translocation of mitochondria to phagosomes, mediated by the assembly of a complex of the ubiquitin ligase TRAF6 and the mitochondrial complex I–assembly factor ECSIT, which results in augmentation of mROS production and bactericidal activity[11]. Furthermore, the heightened innate immune response and increased production of inflammatory cytokines by macrophages from patients with tumor-necrosis factor (TNF) receptor–associated periodic syndrome results from high mROS production rather than high NADPH oxidase–mediated production of ROS[16]. Thus, ROS production by macrophage mitochondria is required for optimal bactericidal activity and innate immune responses. However, how cells achieve the precise temporal and spatial coordination of the induction of phagosomal ROS and mROS is still incompletely understood.

The kinases Mst1 and Mst2 are the closest mammalian homologs of the *Drosophila melanogaster* kinase Hippo, which inhibits cell proliferation and promotes apoptosis during development by inhibiting its downstream effectors Yap and Taz through a kinase cascade formed by the scaffolding proteins WW45 and Mob1 and the kinases Lats1 and Lats2 (refs. 17–30). However, it is less well appreciated that deficiency in Mst1 in humans results in a complex combined immunodeficiency syndrome with recurrent bacterial and viral infections, lymphopenia and variable neutropenia[31,32]. In mice, Mst1 and Mst2 are important regulators of the adhesion, migration, proliferation and apoptosis of

[1]State Key Laboratory of Cellular Stress Biology, Innovation Center for Cell Signaling Network, School of Life Sciences, Xiamen University, Xiamen, China. [2]Department of Laboratory Medicine, the First Affiliated Hospital, Medical College of Xiamen University, Xiamen, China. [3]Institute of Immunology and the CAS Key Laboratory of Innate Immunity and Chronic Disease, Innovation Center for Cell Signaling Network, School of Life Sciences and Medical Center, University of Science and Technology of China, Hefei, China. [4]Department of Biochemistry and Molecular Biology, University of Texas, M.D. Anderson Cancer Center, Houston, Texas, USA. [5]College of Medicine, Chang Gung University, Kwei-Shan, Taiwan. [6]Department of Medicine, Harvard Medical School, Boston, Massachusetts, USA. [7]Department of Molecular Biology, Massachusetts General Hospital, Boston, Massachusetts, USA. [8]These authors contributed equally to this work. Correspondence should be addressed to D.Z. (dwzhou@xmu.edu.cn) or L.C. (chenlanfen@xmu.edu.cn).

Received 29 March; accepted 7 August; published online 28 September 2015; doi:10.1038/ni.3268

T cells[33–41]. However, the role of Mst1 and Mst2 in innate immunity is as yet largely unexplored. Here we found that Mst1 and Mst2 were important for the optimal ROS production and bactericidal activity of phagocytes by promoting activation of the small GTPase Rac and mitochondrial trafficking and juxtaposition to the phagosome through the assembly of a TRAF6-ECSIT complex.

RESULTS

Enhanced susceptibility of Mst1- and Mst2-null mice to sepsis

We used mice with a published hematopoietic cell–specific knockout of Mst1 and Mst2 (*Mst1*$^{-/-}$*Mst2*$^{fl/fl}$*Vav*-Cre mice)[40] to study the role of these kinases in the immune system. The great majority (~70%) of *Mst1*$^{-/-}$*Mst2*$^{fl/fl}$*Vav*-Cre mice exhibited multiple or recurrent infections such as pneumonia (data not shown) and lung abscesses (**Fig. 1a**), as well as unprovoked inflammation in multiple organs, which manifested as colitis and/or glomerulonephritis (**Supplementary Fig. 1a**). We also observed that some mice showed massive extramedullary hematopoiesis and granulopoiesis in the spleen (**Supplementary Fig. 1b,c**). The median survival time for *Mst1*$^{-/-}$*Mst2*$^{fl/fl}$*Vav*-Cre mice was approximately 6 months (data not shown).

The high incidence of bacterial infections in the mice doubly deficient in Mst1 and Mst2 prompted us to investigate the role of Mst1 and Mst2 in the innate immune system, which provides immediate defense against infection by activating phagocytes. We ablated Mst1 and Mst2 in myeloid cells by crossing mice with *lox*P-flanked *Mst1* and *Mst2* alleles (*Mst1*$^{fl/fl}$*Mst2*$^{fl/fl}$) with mice expressing Cre recombinase driven by the myeoid cell–specific promoter of the gene encoding lysozyme M (*Lyz2*-Cre). The resultant *Mst1*$^{fl/fl}$*Mst2*$^{fl/fl}$*Lyz2*-Cre mice with conditional double knockout of *Mst1* and *Mst2* (called 'cDKO mice' here) were born at the expected ratio (data not shown) and exhibited no substantial differences in the number of circulating lymphocytes, monocytes and granulocytes, according to peripheral blood counts, relative to the abundance of these cells in their *Mst1*$^{fl/fl}$*Mst2*$^{fl/fl}$ control littermates (called 'wild-type' mice here) (**Supplementary Fig. 1d**). Flow cytometry indicated that the frequency of Gr-1^{+}CD11b^{+} neutrophils and F480^{+}CD11b^{+} macrophages was much lower in the bone marrow, spleen and blood of cDKO mice than in that of their wild-type littermates, whereas the composition and activation status of T cells and B cells in the spleen, lymph nodes or blood was similar in wild-type and cDKO mice (**Supplementary Fig. 1e,f**).

In contrast to *Mst1*$^{-/-}$*Mst2*$^{fl/fl}$*Vav*-Cre mice, cDKO mice did not show spontaneous inflammation or infections over the first 7 months of life (data not shown). However, in the cecal-ligation-and-puncture (CLP) model of septic peritonitis, the bacterial peritonitis killed ~80% of cDKO mice but only ~40% of their wild-type littermates (**Fig. 1b**). In response to infection, the rapid mobilization of

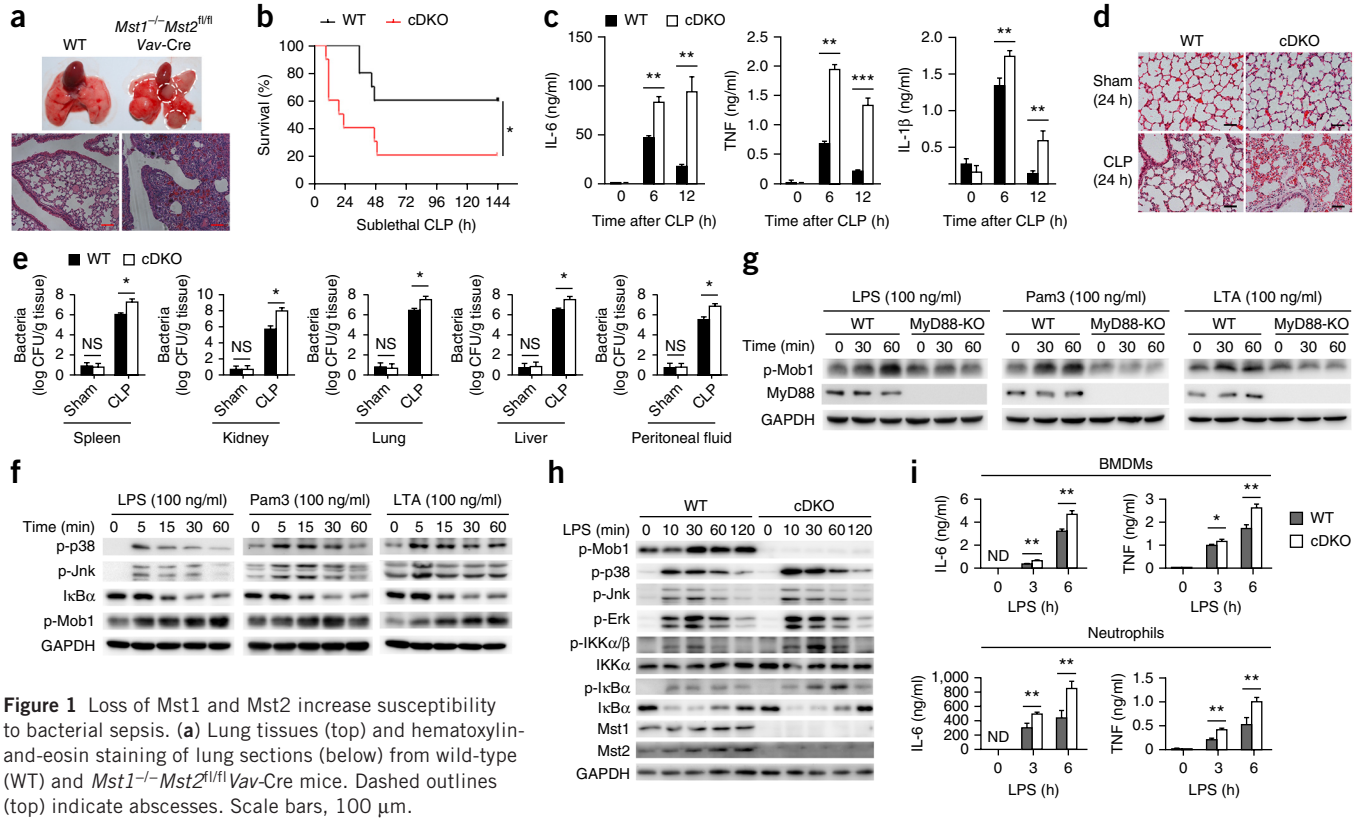

Figure 1 Loss of Mst1 and Mst2 increase susceptibility to bacterial sepsis. (**a**) Lung tissues (top) and hematoxylin-and-eosin staining of lung sections (below) from wild-type (WT) and *Mst1*$^{-/-}$*Mst2*$^{fl/fl}$*Vav*-Cre mice. Dashed outlines (top) indicate abscesses. Scale bars, 100 μm. (**b**–**e**) Mortality (**b**), enzyme-linked immunosorbent assay of serum cytokines (**c**), hematoxylin-and-eosin staining of inflammatory-cell infiltration in the lungs (**d**) and bacterial load (as colony-forming units (CFU)) in the lung, liver, spleen, kidney and peritoneal fluid (**e**) of *Mst1*$^{fl/fl}$*Mst2*$^{fl/fl}$ (WT) or *Mst1*$^{fl/fl}$*Mst2*$^{fl/fl}$*Lyz2*-Cre (cDKO) mice (n = 10 per group per experiment) 24 h after sham treatment or sublethal CLP. Scale bars (**d**), 50 μm. (**f**) Immunoblot analysis of phosphorylated (p-) p38, Jnk and Mob1 and total IκBα and GAPDH (loading control throughout) in wild-type BMDMs stimulated for 0–60 min (above lanes) with LPS, Pam_3CSK_4 (Pam3) or LTA. (**g**) Immunoblot analysis of phosphorylated Mob1 and total MyD88 in wild-type (WT) or MyD88-deficient (MyD88-KO) RAW246.7 cells stimulated for 0, 30 or 60 min (above lanes) with LPS, Pam_3CSK_4 or LTA. (**h**) Immunoblot analysis of wild-type or cDKO BMDMs stimulated for 0–120 min (above lanes) with LPS. (**i**) Enzyme-linked immunosorbent assay of IL-6 and TNF in wild-type and cDKO BMDMs or neutrophils treated for 0, 3 or 6 h with LPS (100 ng/ml). NS, not significant ($P > 0.05$); *$P < 0.05$, **$P < 0.01$ and ***$P < 0.001$ compared with control (Mantel–Cox test (**b**) or Student's t-test (**c**,**e**,**i**)). Data are from one experiment representative of three (**a**–**d**,**f**–**i**) or two (**e**) independent experiments with similar results (mean and s.d. of n = 3 (**c**), n = 5 (**e**) or n = 3 (**i**) biological replicates).

neutrophils and 'emergency' myelopoiesis were similar in the blood of wild-type mice and that of cDKO mice (**Supplementary Fig. 1g**). cDKO mice exhibited significantly higher serum concentrations of the inflammatory cytokines IL-6, TNF and IL-1β at 6 or 12 h after CLP induction than their wild-type littermates (**Fig. 1c**), and had more severe inflammation in lung and kidney tissues at 24 h as well (**Fig. 1d** and **Supplementary Fig. 1h**). In addition, bacterial invasion of the lungs, liver, spleen, kidneys and peritoneal fluid after CLP was significantly higher in cDKO mice than in their wild-type littermates (**Fig. 1e**). These results indicated that the loss of both Mst1 and Mst2 in myeloid cells caused greater susceptibility to bacterial infection and an enhanced inflammatory response.

TLRs induce activation of Mst1 and Mst2 for bacterial clearance

Phagocyte TLRs act as primary sentinels for the detection of pathogens through their binding of microbe-associated molecular patterns, which serve to initiate pro-inflammatory responses[1,2,42,43]. To investigate whether Mst1 and Mst2 participate in TLR-mediated innate host responses to bacterial infections, we stimulated bone marrow–derived macrophages (BMDMs) with an array of TLR ligands, including lipopolysaccharide (LPS) (an agonist of TLR4), the synthetic lipopeptide Pam_3CSK_4 (an agonist of TLR1 and TLR2), lipoteichoic acid (LTA) (an agonist of TLR2), the synthetic RNA duplex poly(I:C) (an agonist of TLR3), the synthetic imidazoquinoline resiquimod (R848) (an agonist of TLR7 and TLR8) and dinucleotide CpG DNA (an agonist of TLR9), and assessed the phosphorylation of Mob1, a physiological substrate of Mst1 and Mst2. We observed that the stimulation of cell-surface TLRs (TLR1, TLR2 and TLR4) substantially enhanced the phosphorylation of Mob1, whereas the ligands of endosomal TLRs (R848 or CpG DNA) did not change the phosphorylation of Mob1, except for a moderate increase in its phosphorylation induced by poly(I:C) (**Fig. 1f** and **Supplementary Fig. 1i**). Through the use of a mouse macrophage-like RAW264.7 cell line deficient in the adaptor MyD88, we further demonstrated that LPS, Pam_3CSK_4 and LTA, derived mainly from bacteria, activated Mst1 and Mst2 via a MyD88-dependent pathway (**Fig. 1g**). We therefore used LPS and Pam_3CSK_4 in subsequent studies as representative stimuli for the activation of Mst1 and Mst2 in phagocytes.

The deletion of Mst1 and Mst2 did not alter the TLR-induced activation of the mitogen-activated protein kinases p38, Jnk or Erk (**Fig. 1h**). However, it resulted in increased induction of pro-inflammatory cytokines, such as IL-6 and TNF, in BMDMs upon stimulation with LPS (**Fig. 1i**). These findings suggested that the greater susceptibility of cDKO mice to CLP-induced bacterial sepsis was not due to a lack of a pro-inflammatory response to bacterial infection.

We then assessed bacterial phagocytosis by incubating fluorescein isothiocyanate (FITC)-labeled *Escherichia coli* or *Listeria monocytogenes* with BMDMs or neutrophils isolated from cDKO mice or their wild-type littermates. Flow cytometry showed that cDKO cells exhibited less phagocytosis of both *E. coli* and *L. monocytogenes* than did wild-type cells (**Fig. 2a**). However, the number of live intracellular bacteria was significantly higher in cDKO BMDMs or neutrophils than in wild-type cells, as measured at late time points (more than 30 min) after bacterial infection (**Fig. 2b**), which indicated that in addition to showing a modest uptake of bacteria, cDKO phagocytes were significantly defective in the intracellular killing of bacteria. Quantification of immunofluorescence micrographs of macrophages incubated with *E. coli* stably expressing green fluorescent protein (GFP–*E. coli*) confirmed that deficiency in Mst1 and Mst2 caused both impaired engulfment of bacteria and defective clearance of bacteria (**Fig. 2c**,**d**). These results indicated that TLR-mediated activation Mst1 and Mst2 was required for phagocytosis and efficient clearance of bacteria.

Deletion of Mst1 and Mst2 results in impaired mROS induction

ROS have an essential role in bacterial killing by phagocytes[4,12]. In addition to phagosomal NADPH-oxidase, mROS are an essential source of ROS in this process. Through the use of ROS-sensitive dyes (mitoSOX to measure the mROS superoxide, and CM-H2DCFDA or CellROX to measure total cellular H_2O_2) and flow cytometry, we observed that unstimulated wild-type and cDKO BMDMs had the same amount of mROS, whereas the basal amount of total cellular ROS was moderately greater in cDKO cells than in wild-type cells (**Fig. 2e**). To measure phagosomal ROS, we coupled *E. coli* with CellROX, as well as with the DNA-binding dye DAPI, for visualization. We labeled wild-type BMDMs with the division-tracking dye CFSE and mixed them with unlabeled cDKO BMDMs, or vice versa, then infected the mixed cells with CellROX-DAPI–coupled *E. coli*. Our data showed that the induction of phagosomal ROS was considerably impaired in cDKO BMDMs after bacterial infection (**Fig. 2f**).

As reported above, engagement of the cell-surface TLRs (TLR1, TLR2 and TLR4) augmented mROS and total cellular ROS in BMDMs and neutrophils, but engagement of the endosomal TLRs (TLR3, TLR7, TLR8 and TLR9) did not (**Fig. 2g** and **Supplementary Fig. 2a**). Notably, stimulation of TLR1, TLR2 or TLR4 on cDKO BMDMs or neutrophils with their ligands caused little or no increase in mROS and total cellular ROS compared with their abundance in wild-type cells (**Fig. 2g** and **Supplementary Fig. 2a**), and infection with whole bacteria also yielded substantially lower concentrations of total ROS in cDKO cells than in their wild-type counterparts (**Fig. 2h** and **Supplementary Fig. 2b**). We therefore investigated whether the considerably diminished induction of mROS in cDKO cells was due to a reduced ability of their mitochondria to generate ROS. In contrast, we found that rotenone, oligomycin and antimycin A, which are electron-transport inhibitors known to increase mitochondrial generation of superoxide, augmented mROS production to a similar extent in wild-type and cDKO BMDMs (**Supplementary Fig. 2c**). In addition, the number of mitochondria, the main electron-transport-chain components and the mitochondrial membrane potential were also similar in wild-type and cDKO cells (**Supplementary Fig. 2d–f**). Thus, a lack of Mst1 and Mst2 did not diminish the capacity of mitochondria for ROS production, and some other factors might have been responsible for the impaired phagosomal mROS production.

Mst1 and Mst2 control the mitochondrion-phagosome juxtaposition

We next investigated how deficiency in Mst1 and Mst2 would affect the induction of mROS in phagocytes after the activation of TLR1, TLR2 or TLR4. Because mitochondria are recruited to phagosomes containing intracellular pathogens[11], we investigated whether this process was impaired in cDKO phagocytes. We incubated BMDMs with latex beads coated with microbe-associated molecular patterns to elicit phagocytosis of the beads by the cells, which enabled visualization of the juxtaposition of phagosomes to mitochondria. cDKO BMDMs displayed much less mitochondrial cupping around phagocytosed Pam_3CSK_4- or LPS-coated beads than did wild-type BMDMs (**Fig. 3a**). In addition, many more bacteria localized together with the mitochondria in wild-type BMDMs than in cDKO cells during infection with GFP–*E. coli* (**Fig. 3b**).

Mst1 deficiency in T cells causes cytoskeletal disorganization[39,40]. Similarly, we found that cDKO BMDMs exhibited disrupted F-actin organization compared with its organization in wild-type cells (**Fig. 3c**). To determine whether such cytoskeletal reorganization

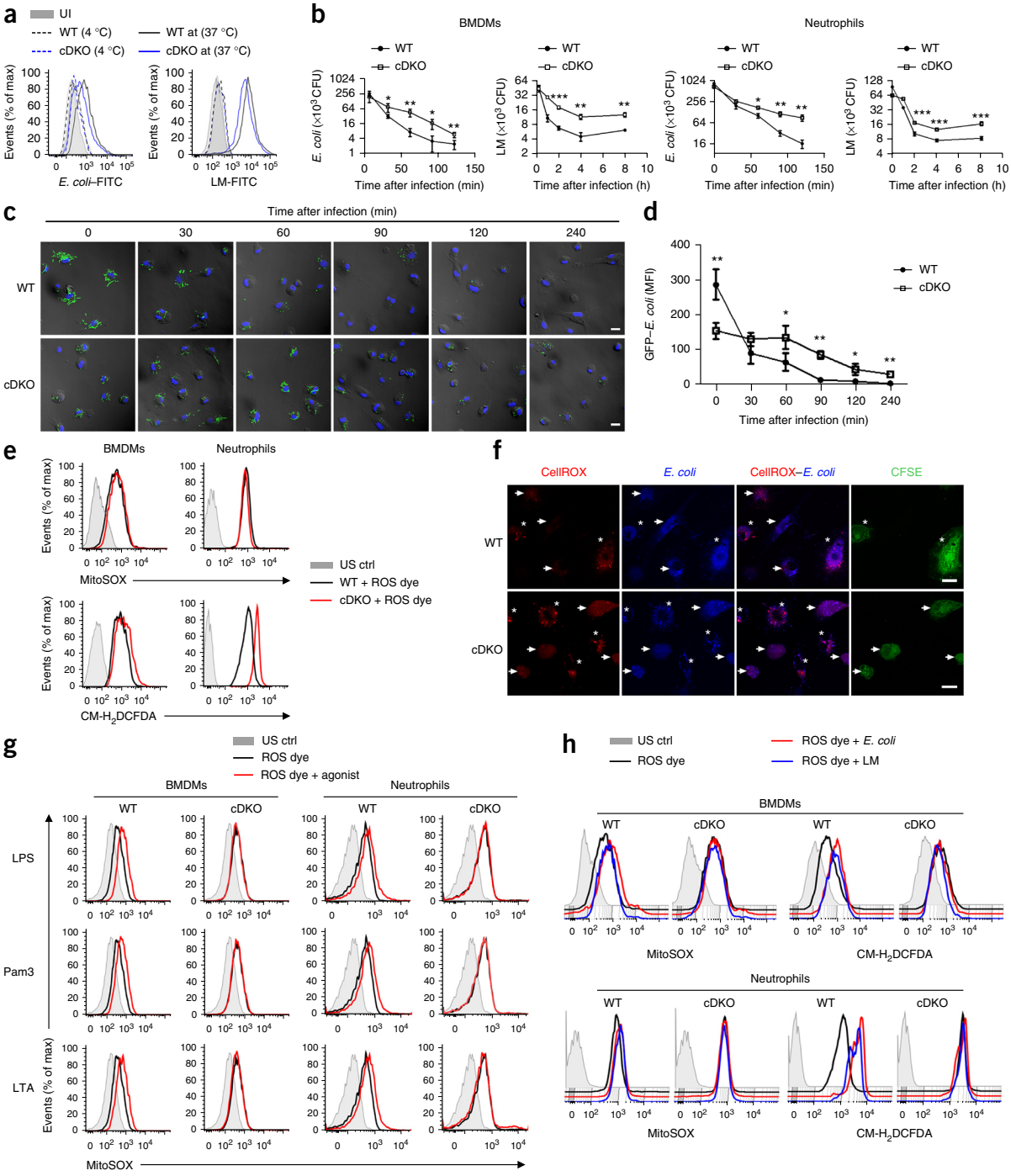

Figure 2 Mst1- and Mst2-deficient myeloid cells are defective in killing bacteria and in the induction of ROS. (**a**) Flow cytometry of wild-type and cDKO BMDMs left uninfected (UI) or infected for 20 min at 37 °C or 4 °C (key) with FITC-labeled *E. coli* (*E. coli*-FITC) at a multiplicity of infection (MOI) of 20 or with FITC-labeled *L. monocytogenes* (LM-FITC) at an MOI of 10. (**b**) Pathogen burden in wild-type and cDKO BMDMs or neutrophils infected with *L. monocytogenes* (MOI, 10) or *E. coli* (MOI, 20), presented as colony-forming units (CFU). (**c**) Fluorescence microscopy of wild-type and cDKO BMDMs infected for 0–240 min (above images) with GFP–*E. coli* (green), then washed, fixed and stained with the DNA-binding dye DAPI (blue). Scale bars, 20 μm. (**d**) Quantification of the results in **c**, presented as mean fluorescence intensity (MFI). (**e**) Flow cytometry of wild-type BMDMs left unstained, as a control (US ctrl), or of wild-type and cDKO BMDMs or neutrophils stained for 30 min with the ROS dye MitoSOX (mROS) or CM-H_2DCFDA (cellular ROS). (**f**) Fluorescence microscopy of phagosomal ROS in wild-type BMDMs (top) or cDKO BMDMs (bottom) labeled with CFSE, then mixed with unlabeled cDKO cells (*) or wild-type BMDMs (arrows) and CellROX- and DAPI-coupled *E. coli*. Scale bars, 20 μm. (**g**) Flow cytometry analyzing mROS production by unstimulated wild-type BMDMs left unstained (US ctrl) or by wild-type and cDKO BMDMs or neutrophils left unstimulated (ROS dye) or stimulated for 6 h with the TLR agonist LPS, Pam_3CSK_4 or LTA (ROS dye + agonist), then stained for 30 min with MitoSOX. (**h**) Flow cytometry analyzing the production of mROS and cellular ROS (as in **e**) in uninfected wild-type BMDMs left unstained (US ctrl) or in wild-type and cDKO BMDMs or neutrophils infected *E. coli* or *L. monocytogenes* and then stained for 30 min with MitoSOX or CM-H_2DCFDA. $^*P < 0.05$, $^{**}P < 0.01$ and $^{***}P < 0.001$, wild-type versus cDKO at the same time point (Student's *t*-test). Data are from one experiment representative of three (**a**–**e**,**g**,**h**) or two (**f**) independent experiments with similar results (mean ± s.d. of $n = 5$ biological replicates in **b**,**d**).

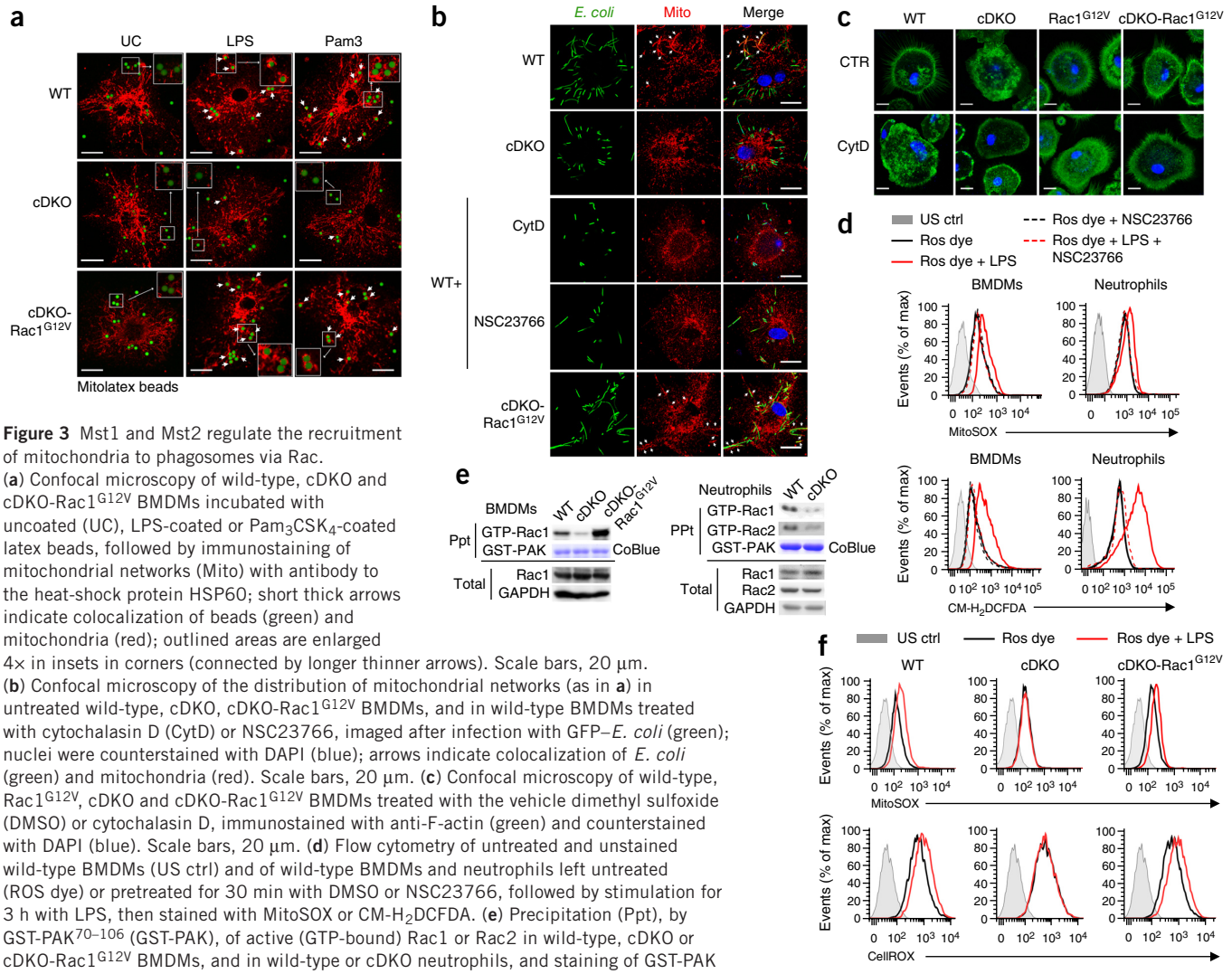

Figure 3 Mst1 and Mst2 regulate the recruitment of mitochondria to phagosomes via Rac. (**a**) Confocal microscopy of wild-type, cDKO and cDKO-Rac1^{G12V} BMDMs incubated with uncoated (UC), LPS-coated or Pam_3CSK_4-coated latex beads, followed by immunostaining of mitochondrial networks (Mito) with antibody to the heat-shock protein HSP60; short thick arrows indicate colocalization of beads (green) and mitochondria (red); outlined areas are enlarged 4× in insets in corners (connected by longer thinner arrows). Scale bars, 20 μm. (**b**) Confocal microscopy of the distribution of mitochondrial networks (as in **a**) in untreated wild-type, cDKO, cDKO-Rac1^{G12V} BMDMs, and in wild-type BMDMs treated with cytochalasin D (CytD) or NSC23766, imaged after infection with GFP–*E. coli* (green); nuclei were counterstained with DAPI (blue); arrows indicate colocalization of *E. coli* (green) and mitochondria (red). Scale bars, 20 μm. (**c**) Confocal microscopy of wild-type, Rac1^{G12V}, cDKO and cDKO-Rac1^{G12V} BMDMs treated with the vehicle dimethyl sulfoxide (DMSO) or cytochalasin D, immunostained with anti-F-actin (green) and counterstained with DAPI (blue). Scale bars, 20 μm. (**d**) Flow cytometry of untreated and unstained wild-type BMDMs (US ctrl) and of wild-type BMDMs and neutrophils left untreated (ROS dye) or pretreated for 30 min with DMSO or NSC23766, followed by stimulation for 3 h with LPS, then stained with MitoSOX or CM-H_2DCFDA. (**e**) Precipitation (Ppt), by GST-PAK$^{70–106}$ (GST-PAK), of active (GTP-bound) Rac1 or Rac2 in wild-type, cDKO or cDKO-Rac1^{G12V} BMDMs, and in wild-type or cDKO neutrophils, and staining of GST-PAK with Coomassie blue (CoBlue); below, immunoblot analysis of total Rac1 and Rac2 in the cells above. (**f**) Flow cytometry of unstimulated and unstained wild-type BMDMs (US ctrl) and of wild-type, cDKO or cDKO-Rac1^{G12V} BMDMs stimulated for 3 h with LPS, then left unstained or stained with MitoSOX or CellRox. Data are from one experiment representative of three independent experiments with similar results (**a**–**f**), with 8~100 cells (**a**–**c**).

was required for the juxtaposition of phagosomes and mitochondria in macrophages, we treated wild-type BMDMs with cytochalasin D. As expected, this inhibitor of F-actin disrupted the cytoskeleton in a manner similar to that observed in cDKO BMDMs (**Fig. 3c** and **Supplementary Fig. 3a**) and significantly reduced the co-localization of GFP–*E. coli* with mitochondria (**Fig. 3b**), as well as the induction of mROS upon stimulation with LPS (**Supplementary Fig. 3b**). Mst1 and Mst2 regulate chemokine-stimulated reorganization of F-actin in thymocytes by promoting activation of the small GTPase Rac[40]. Treatment of BMDMs with the Rac inhibitor NSC23766 decreased the co-localization of mitochondria with GFP–*E. coli* (**Fig. 3b**) and blocked the LPS-stimulated increase in both mROS and total cellular ROS in BMDMs and neutrophils (**Fig. 3d**).

Although the overall abundance of Rac in cDKO BMDMs and neutrophils was similar to that in wild-type cells, the amount of Rac-GTP was much lower in the mutant cells, as estimated by precipitation with a glutathione *S*-transferase (GST)-tagged fragment (residues 70–106) of the kinase PAK (PAK$^{70–106}$) (**Fig. 3e**). To determine whether the impaired recruitment of mitochondria in cDKO BMDMs was caused by defective activation of Rac, we crossed cDKO mice with R26Stop^{FL}RACDA mice, which have inducible expression of a constitutively active form of Rac1 (Rac1^{G12V}), to generate 'cDKO-Rac1^{G12V}' mice. These mice expressed constitutively active Rac1^{G12V} in cDKO myeloid lineages (**Fig. 3e**). BMDMs from cDKO-Rac1^{G12V} mice displayed normal organization of F-actin (**Fig. 3c** and **Supplementary Fig. 3a**), normal mitochondrion-phagosome juxtaposition (**Fig. 3a**,**b**) and normal production of mROS and cellular ROS upon stimulation with LPS (**Fig. 3f**). These results indicated that the activation of Rac by Mst1 and Mst2 was critical for innate host defense by positively regulating the recruitment of mitochondria to phagosomes for optimal induction of mROS.

Mst1 and Mst2 disrupt the LyGDI-Rac complex via PKC-α

We next investigated the mechanism by which Mst1 and Mst2 regulated Rac activity in phagocytes. The precipitation of Flag-tagged Mst2 transiently expressed in RAW264.7 cells retrieved several endogenous proteins selectively, as identified by mass spectrometry, including PKC proteins and LyGDI (**Fig. 4a**). LyGDI belongs to a family of three Rho-GDP–dissociation inhibitors that bind Rac-GDP in a cytosolic complex. The PKC-α-mediated phosphorylation of LyGDI at Ser31 disrupts the interaction between LyGDI and Rac; this releases Rac-GDP, which translocates to the membrane and undergoes guanyl

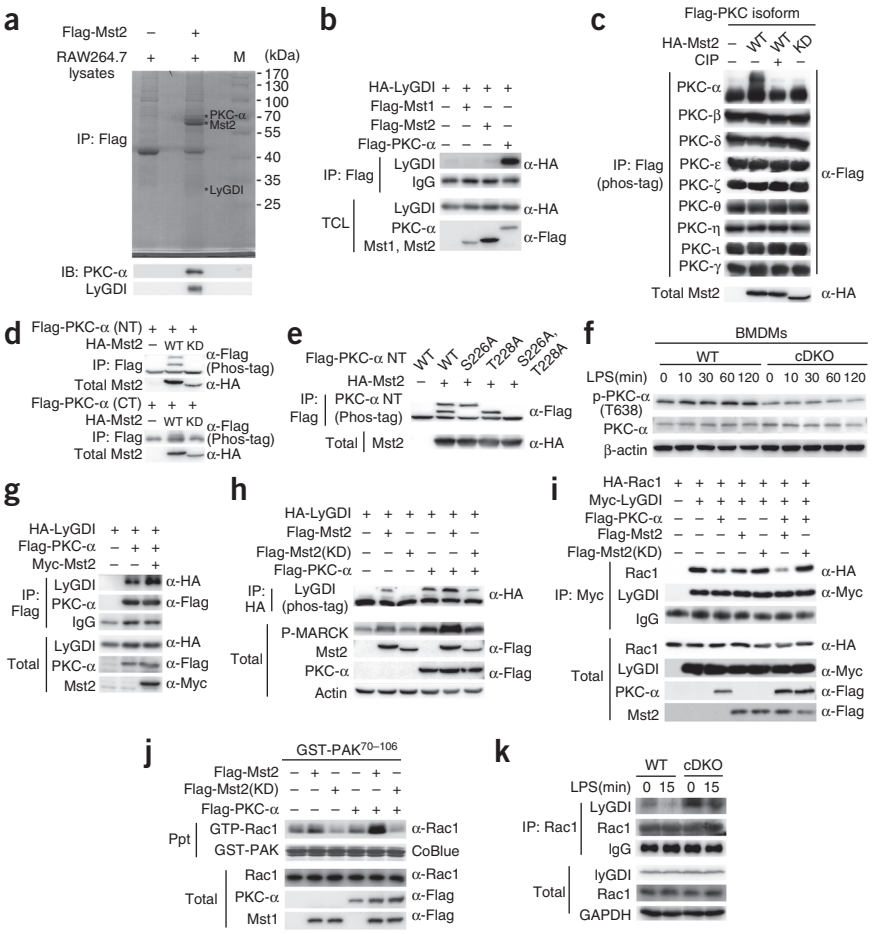

Figure 4 Mst1 and Mst2 regulate the activation of Rac through PKC-LyGDI. (**a**) Identification of LyGDI and PKC-α by mass spectrometry in a Flag-tagged Mst2-precipitation assay of RAW264.7 cell lysates. *, migration of PKC-α, Mst2 or LyGDI; IP, immunoprecipitation; IB, immunoblot analysis; M, molecular size markers. (**b**) Immunoassay of lysates of 293T cells expressing various combinations (above lanes) of HA-tagged LyGDI and Flag-tagged Mst1, Mst2 or PKC-α, immunoprecipitated with anti-Flag and analyzed by immunoblot with anti-HA (α-HA) or anti-Flag (α-Flag) (right margin); below, immunoblot analysis of total cell lysates (TCL) without immunoprecipitation. (**c**) Phos-tag and SDS-PAGE analysis of Flag-tagged PKC-α, PKC-β, PKC-γ, PKC-δ, PKC-ε, PKC-η, PKC-θ, PKC-ι or PKC-ζ expressed together with HA-tagged wild-type Mst2 (WT) or kinase-inactive Mst2 (KD) in 293T cells left untreated (CIP –) or treated calf intestinal alkaline phosphatase (CIP +), immunoprecipitated with anti-Flag–conjugated beads. (**d**) Phos-tag analysis (as in **c**) of 293T cells expressing empty vector (–) or HA-tagged wild-type or kinase-inactive Mst2, plus a Flag-tagged amino-terminal (NT) fragment of PKC-α (residues 1–338) (top) or carboxy-terminal (CT) fragment of PKC-α (residues 339–672) (bottom). (**e**) Phos-tag analysis (as in **c**) of 293T cells expressing Flag-tagged wild-type PKC-α or PKC-α(S226A), PKC-α(T228A) or PKC-α(S226A,T228A) and HA-tagged Mst2 (above lanes). (**f**) Immunoblot analysis of PKC-α phosphorylated at Thr638 (PKC-α(T638)), total PKC-α and β-actin (loading control throughout) in lysates of wild-type and cDKO BMDMs stimulated for 0–120 min (above lanes) with LPS. (**g**) Immunoassay (as in **b**) of 293T cells expressing various combinations (above lanes) of HA-tagged LyGDI, Flag-tagged PKC-α and Myc-tagged Mst2. (**h**) Phos-tag analysis (as in **c**) of 293T cells expressing various combinations (above lanes) of HA-tagged LyGDI, Flag-tagged PKC-α and wild-type or kinase-inactive Mst2. (**i**) Immunoassay (as in **b**) of 293T cells expressing various combinations (above lanes) of HA-tagged Rac1, Myc-tagged LyGDI and Flag-tagged PKC-α and wild-type or kinase-inactive Mst2, immunoprecipitated with anti-Myc. (**j**) GST-precipitation assay (as in **Fig. 3e**) of endogenous active (GTP-bound) Rac in 293T cells expressing various combinations (above lanes) of Flag-tagged PKC-α and wild-type or kinase-inactive Mst2, detected with anti-Rac1. (**k**) Immunoblot analysis of total lysates (bottom) and immunoprecipitates (top) of wild-type and cDKO BMDMs treated for 0 or 15 min with LPS. Data are from one experiment representative of three independent experiments with similar results.

nucleotide exchange[6]. Although neither Mst1 nor Mst2 bound directly to LyGDI, PKC-α did bind strongly to LyGDI (**Fig. 4b**). Transiently expressed hemagglutinin (HA)-tagged Mst2 (HA-Mst2) bound to various co-expressed Flag-tagged PKC isoforms (PKC-α, PKC-β, PKC-γ, PKC-δ, PKC-ε, PKC-η, PKC-θ, PKC-ι and PKC-ζ; **Supplementary Fig. 4a**); however, only PKC-α migrated more slowly and produced an 'up-shifted' band (as visualized by the Phos-tag labeling system for the analysis of phosphorylation, followed by SDS-PAGE) when co-expressed with wild-type Mst2, but it did not do so when co-expressed with a kinase-inactive form of Mst2 (**Fig. 4c**), which indicated that PKC-α was a substrate of Mst2. Mst2-mediated phosphorylation of PKC-α, as well as the Mst2-binding site, was on the amino-terminal regulatory domain of PKC-α (**Fig. 4d** and **Supplementary Fig. 4b**). Mass spectrometry and site-directed mutagenesis further revealed that PKC-α was phosphorylated by Mst2 at Ser226 and Thr228 (**Fig. 4e** and **Supplementary Fig. 4c**). The LPS-stimulated increase in the phosphorylation of PKC-α at Thr638, an autophosphorylation site reflective of PKC-α activation, was much lower in cDKO BMDMs than in wild-type BMDMs (**Fig. 4f**). Thus, phosphorylation of PKC-α at Ser226 and Thr228 by Mst1 and Mst2 was required for the optimal activation of PKC-α. Consistent with that, co-expression of PKC-α with Mst2 enhanced the interaction between PKC-α and LyGDI (**Fig. 4g**), and this in turn promoted the phosphorylation of LyGDI by PKC-α (**Fig. 4h**). The phosphorylation of LyGDI led to its dissociation from the LyGDI-Rac1 complex (**Fig. 4i**), which augmented the 'charging' of Rac-GTP (**Fig. 4j**). In confirmation of the results obtained by transfection, the ability of LPS to diminish the interaction between LyGDI and Rac1 was much lower in cDKO BMDMs than in wild-type BMDMs (**Fig. 4k**). These results established that Mst1 and Mst2, via the activation of PKC-α, disrupted the LyGDI-Rac interaction to promote activation of Rac.

TLR signaling induces the TRAF6-mediated Rac ubiquitination

As shown above (**Fig. 3b**), the infection of wild-type BMDMs with *E. coli* promoted the co-localization of phagocytosed bacteria with mitochondria, a response that was lost in cDKO BMDMs but was restored by the expression of a constitutively active form of Rac ($Rac1^{G12V}$). Moreover, infection of wild-type BMDMs with *E. coli* increased the co-localization of Rac with phagosomes, and this response was much lower in cDKO BMDMs and in wild-type BMDMs treated with the Rac inhibitor NSC23766 (**Supplementary Fig. 5a**). To identify candidate Rac effectors of signaling after bacterial infection, we incubated purified Flag-tagged $Rac1^{G12V}$ or an inactive form of Rac ($Rac1^{T17N}$) with extracts of BMDMs and

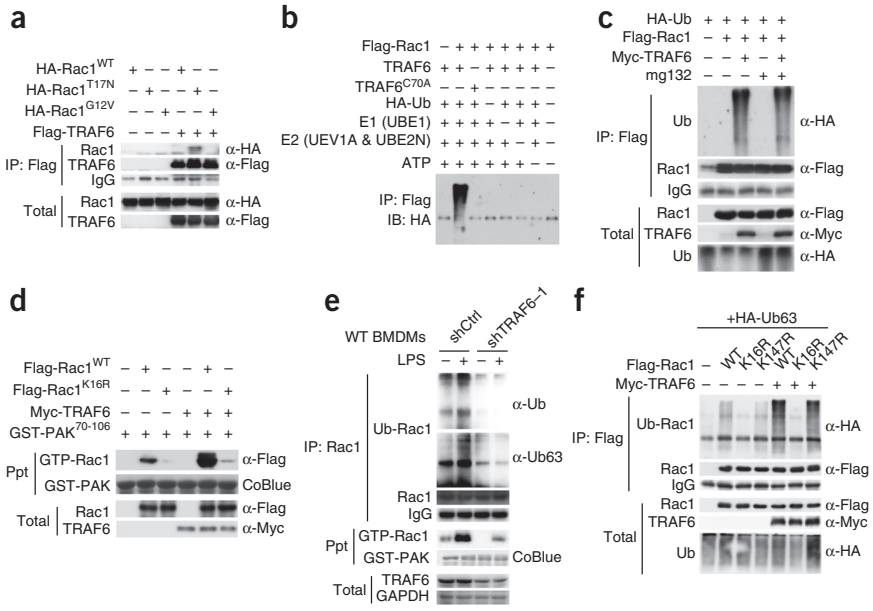

Figure 5 TRAF6 positively regulates the Lys63-linked ubiquitination of Rac1 *in vitro* and *in vivo*. (**a**) Immunoblot analysis of total lysates (bottom) and anti-Flag immunoprecipitates (top) of 293T cells expressing various combinations (above lanes) of HA-tagged wild-type Rac1, HA-Rac1^{G12V} or HA-Rac1^{T17N} and Flag-tagged TRAF6. (**b**) *In vitro* ubiquitination assay of various combinations (above lanes) of Flag-tagged recombinant Rac1, wild-type TRAF6 or catalytically inactive TRAF6^{C70A}, plus the components HA-tagged ubiquitin (HA-Ub), E1 (UBE1), the E2 complex (UEV1A & UBE2N) and ATP. (**c**) Immunoassay (as in **a**) of the ubiquitination of Rac (detected with anti-HA) in 293T cells expressing various combinations (above lanes) of Flag-tagged Rac1, Myc-tagged TRAF6 and HA-tagged ubiquitin, treated with DMSO (MG132 –) or the proteasome inhibitor MG132 (MG132 +). IgG, control antibody immunoglobulin G (throughout). (**d**) Immunoblot analysis of the association of active (GTP-bound) Rac1 with GST-PAK$^{70–106}$ in lysates of 293T cells expressing various combinations (above lanes) of Flag-tagged wild-type Rac1 or Rac1^{K16R} and Myc-tagged TRAF6, incubated with GST-PAK$^{70–106}$ (GST-PAK); CoBlue (middle), staining of GST-PAK$^{70–106}$ with Coomassie blue. (**e**) Immunoblot analysis of K63-linked polyubiquitination (Ub63) of Rac1 in immunoprecipitates and total lysates of wild-type BMDMs treated with control shRNA (shCtrl) or TRAF6-specific shRNA (shTRAF6-1), left untreated (–) treated (+) for 15 min with LPS (100 ng/ml). (**f**) Immunoblot analysis of Rac1 ubiquitination (Ub-Rac1) in 293T cells expressing various combinations (above lanes) of Flag-tagged wild-type Rac1, Rac1^{K16R} or Rac1^{K147R} and Myc-tagged TRAF6. Data are from one experiment representative of three independent experiments with similar results.

identified, by mass spectroscopy, the endogenous proteins purified together by immunoprecipitation with antibody to Flag (anti-Flag). Among the proteins identified was the E3 ubiquitin ligase TRAF6, a key intermediate in TLR signaling, that specifically precipitated together with Flag-Rac1^{T17N} but not with Flag-Rac1^{G12V} (**Supplementary Fig. 5b**). We confirmed the selective interaction of TRAF6 with inactive Rac1^{T17N}, but not with active Rac1^{G12V}, by transfection of vector encoding Flag-TRAF6 together with vector encoding HA-tagged wild-type Rac1, Rac1^{T17N} (i.e., Rac-GDP) or Rac1^{G12V} (i.e., Rac-GTP) into 293T human embryonic kidney cells, followed by immunoprecipitation with anti-Flag (**Fig. 5a**).

TRAF6 functions with the ubiquitin-conjugating (E2) complex (consisting of UEV1A and UBE2N) to catalyze the synthesis of Lys63 (K63)-linked polyubiquitin chains on target proteins, including TRAF6 itself[44]. The incubation of Rac1 with TRAF6 and standard components required for *in vitro* ubiquitination demonstrated the ability of TRAF6 to catalyze the ubiquitination of Rac1 (**Fig. 5b**). Substitution of a cysteine residue (Cys70) in the RING domain of TRAF6 (required for its E3 ligase activity) abolished the ubiquitination of Rac1 (**Fig. 5b**). Furthermore, transfection of vectors encoding TRAF6 and Rac1 with vector encoding HA-tagged wild-type ubiquitin or ubiquitin variants that permit only K63 or K48 linkage established that the TRAF6-catalyzed polyubiquitination of Rac1 was exclusively K63 linked (**Supplementary Fig. 5c**). Consistent with the lack of K48-linked ubiquitination, the proteasome inhibitor MG132 did not increase the amount of ubiquitinated Rac (**Fig. 5c**). TRAF6 catalyzed the ubiquitination of Rac1 and enhanced the activation state of Rac1 (**Fig. 5d**). The downregulation of endogenous TRAF6 expression in BMDMs and RAW264.7 cells through the use of short hairpin RNA (shRNA) (**Supplementary Fig. 5d**) was accompanied by a marked reduction in total and K63-linked ubiquitination of Rac and activation of Rac in resting and LPS-stimulated BMDMs (**Fig. 5e**).

To map the ubiquitin acceptor site(s) in Rac1, we individually replaced each of the 17 lysine residues in the Rac1 sequence with arginine and measured the ubiquitination of these Rac1 variants in 293T cells (**Supplementary Fig. 5e**). Only the mutant with the K16R substitution (Rac1^{K16R}) underwent substantially less polyubiquitination than did wild-type Rac1, whereas several other mutants, such as Rac1^{K147R}, exhibited a relatively small reduction in polyubiquitination (**Supplementary Fig. 5c**). The transfection of 293T cells with vector expressing Flag-tagged Rac1^{K16R} or Rac1^{K147R} together with vector expressing Myc-tagged TRAF6 demonstrated that Lys16 was the ubiquitin acceptor site (**Fig. 5f**) and was required for the TRAF6-induced activation of Rac1 (**Fig. 5d**). These results established that TRAF6 directly bound to Rac and catalyzed K63-linked polyubiquitination of Rac at Lys16 *in vitro* and *in vivo*.

TRAF6-mediated ubiquitination is crucial for Rac activation

We observed that endogenous TRAF6 bound selectively to Rac1^{T17N}, rather than to wild-type Rac1 or Rac1^{G12V} (**Fig. 5a**), and localized together with Rac1^{T17N}, but not with Rac1^{G12V}, at the cell periphery (**Supplementary Fig. 6a**). In contrast, GST-TRAF6 bound to Rac1 *in vitro* to a similar extent whether Rac1 was 'charged' with GDP or GTP (**Fig. 6a**). Conversely, unlike the association of wild-type TRAF6 with Rac1 variants, the association of catalytically inactive TRAF6^{C70A} with wild-type Rac1, Rac1^{T17N} or Rac1^{G12V} in 293T cells was comparable (**Fig. 6b**). We therefore sought to define the effect of the guanylnucleotide 'charging' of Rac1 on its ability to undergo ubiquitination by TRAF6. Myc-tagged TRAF6 expressed in 293T cells ubiquitinated co-expressed wild-type Rac1 and, to a greater extent, Rac1^{G12V}, but was unable to ubiquitinate Rac1^{T17N} (**Fig. 6c**). In addition, the Rac1 inhibitor NSC23766 diminished the ubiquitination of Rac1 by coexpressed TRAF6 (**Supplementary Fig. 6b**). *In vitro*, loading of Rac1 with GTPγS (a nonhydrolyzable GTP) was required for TRAF6-catalyzed ubiquitination, whereas Mg^{2+}-free and inactive Rac1-GDP were both resistant to ubiquitination (**Fig. 6d**). The impaired activation of endogenous Rac observed in cDKO BMDMs (**Fig. 3e**) was paralleled by less ubiquitination of Rac in LPS-stimulated cDKO BMDMs

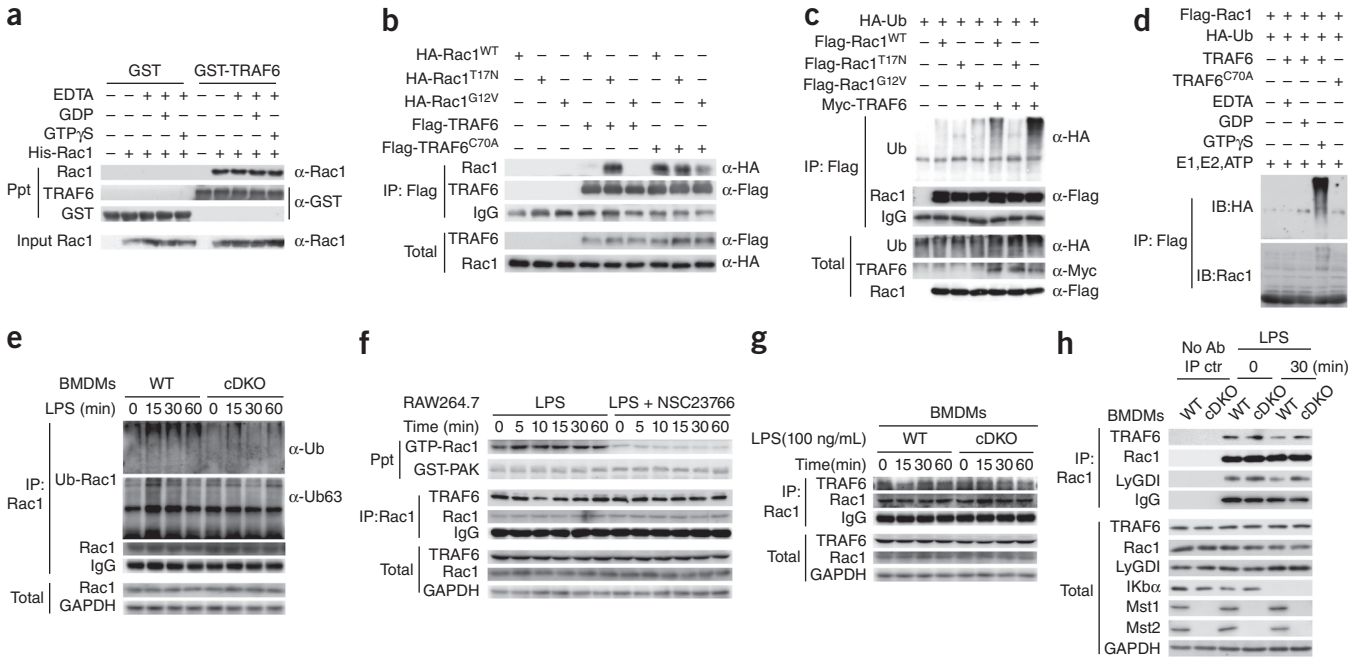

Figure 6 TRAF6 maintains Rac1 in an activated state via K63-linked ubiquitination. (**a**) Immunoblot analysis of the precipitation of TRAF6 with HACE1 (E3 ubiquitin ligase)-associated Rac1 *in vitro* among beads coupled to GST or GST-TRAF6 incubated with various combinations (above lanes) of recombinant purified histidine (His)-tagged Rac1, a Mg^{2+}-free form of Rac1 (EDTA) or Rac1 loaded with GDP or GTPγS; below, immunoblot analysis of input Rac1. (**b**) Immunoblot analysis of total lysates (bottom) and anti-Flag immunoprecipitates (top) in 293T cells expressing various combinations (above lanes) of HA-tagged wild-type Rac1, $Rac1^{G12V}$ or $Rac1^{T17N}$ and Flag-tagged TRAF6 or Flag-$TRAF6^{C70A}$. (**c**) Immunoassay (as in **b**) of the ubiquitination of active Rac1 by TRAF6 in 293T cells expressing various combinations (above lanes) of Flag-tagged wild-type Rac1, $Rac1^{G12V}$ or $Rac1^{T17N}$ and Myc-tagged TRAF6. (**d**) *In vitro* assay of the ubiquitination, by TRAF6, of recombinant Rac1 loaded with GTPγS or GDP or the Mg^{2+}-free form of Rac1 (EDTA). (**e**) Immunoblot analysis of Rac1 ubiquitination in total lysates (bottom) and immunoprecipitates (top) of wild-type and cDKO BMDMs treated for 0–60 min (above lanes) with LPS (100 ng/ml), probed with anti-ubiquitin (α-Ub) and antibody to K63-linked ubiquitin (α-Ub63). (**f**,**g**) Immunoblot analysis of the association of active (GTP-bound) Rac1 with GST-$PAK^{70–106}$ (**f**) and the association of TRAF6 and Rac1 (**f**,**g**) in total lysates (bottom) and anti-Rac1 immunoprecipitates (top) of RAW264.7 cells treated for 0–60 min (above lanes) with LPS or LPS plus NSC23766 (**f**) and wild-type or cDKO BMDMs treated for 0–60 min (above lanes) with LPS (**g**). (**h**) Immunoblot analysis of the association of Rac1, TRAF6 and LyGDI in total lysates (bottom) and anti-Rac1 immunoprecipitates (top) of wild-type and cDKO BMDMs stimulated for 0 or 30 min (above lanes) with LPS; far left (No Ab IP ctrl), samples treated with protein G beads without the addition of anti-Rac1. Data are from one experiment representative of three independent experiments with similar results.

than in wild-type BMDMs (**Fig. 6e**). Thus, TRAF6 'preferentially' ubiquitinated the 'GTP-charged' active form of Rac.

The stimulation of RAW264.7 cells with LPS increased the GTP 'charging' of Rac and was accompanied by a decrease in the association of Rac with TRAF6 (**Fig. 6f**). The inhibition of the GTP 'charging' of Rac by NSC23766, although it diminished the ubiquitination of Rac (**Supplementary Fig. 6b**), prevented the LPS-induced dissociation of TRAF6 from Rac1 (**Fig. 6f**). Stimulation of wild-type BMDMs with LPS also reduced the association of Rac1 with TRAF6 (**Fig. 6g**) and with LyGDI (**Fig. 6h**), which did not occur in LPS-stimulated cDKO BMDMs (**Fig. 6g**,**h**). These results indicated that the LPS induced the release of Rac-GDP from LyGDI by initiating GTP 'charging' of Rac1, which enabled the TRAF6-catalyzed, K63-linked polyubiquitination of Rac-GTP at Lys16, followed by the dissociation of TRAF6 from Rac-GTP. The ubiquitination of Rac, although it was catalyzed subsequent to 'charging' of Rac1 with GTP, augmented and presumably stabilized such 'charging'. These results established that TRAF6-mediated, K63-linked ubiquitination further enhanced the GTP 'charging' and activation of Rac.

Active Rac promotes assembly of the TRAF6-ECSIT complex

The recruitment of mitochondria to phagosomes and increased mROS production are mediated by the assembly of a complex of TRAF6 with ECSIT in the mitochondria[11]. We found that after infection of BMDMs with *E. coli*, the co-localization of TRAF6 and ECSIT with the bacteria that occurred in wild-type cells did not occur in cDKO cells, and this defect was 'rescued' in cDKO-$Rac1^{G12V}$ BMDMs (**Fig. 7a**). To investigate how GTP-bound Rac1 promoted assembly of the TRAF6-ECSIT complex, we performed precipitation assays to determine the relationships of these three molecules. ECSIT interacted with the carboxy-terminal MATH domain (amino acids 351–522) of TRAF6 (**Supplementary Fig. 7a**), which was the same region of TRAF6 that bound to Rac1 (**Supplementary Fig. 7b**,**c**). Co-expression of TRAF6 and ECSIT with Rac1 variants showed that wild-type Rac1 only modestly displaced ECSIT from TRAF6, but inactive $Rac1^{T17N}$ did so substantially (**Fig. 7b**). Furthermore, $Rac1^{G12V}$ had little or no effect on the TRAF6-ECSIT complex (**Fig. 7b**). Immunofluorescence staining further confirmed that active Rac1 greatly enhanced the co-localization of ECSIT and TRAF6 in HeLa cells, but inactive Rac1 did not (**Supplementary Fig. 7d**). These data indicated that the tight interaction of TRAF6 with inactive Rac1 was probably due to inefficient ubiquitination of inactive Rac1 by TRAF6. Thus, inactive Rac acted in a dominant-negative fashion to block the association of TRAF6-ECSIT through the competitive binding of ECIST and inactive Rac to TRAF6.

The inactivating $Rac2^{D57N}$ substitution causes a human immunodeficiency syndrome characterized by a substantial reduction in ROS production in phagocytes[8–10]. We found that as with

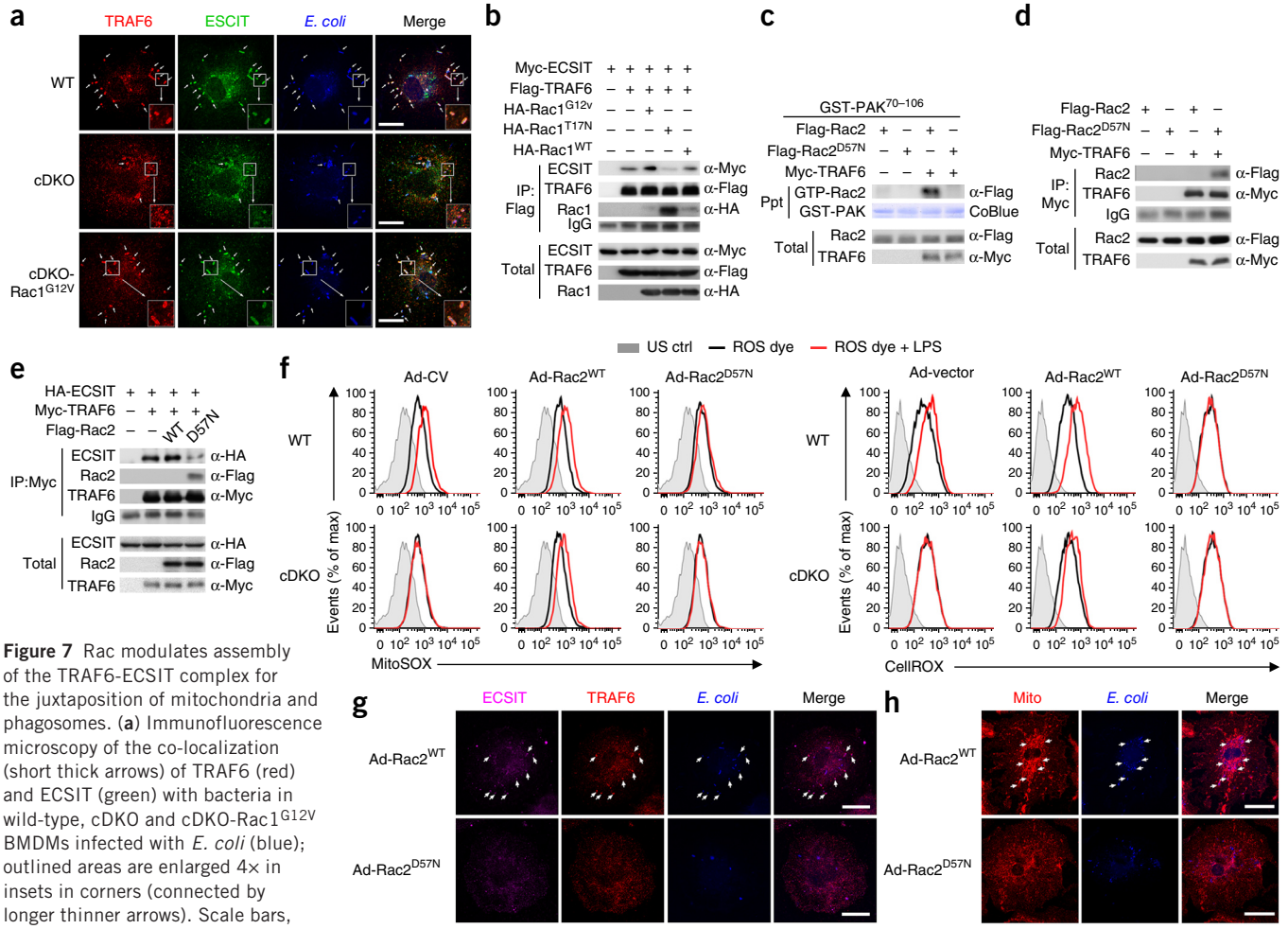

Figure 7 Rac modulates assembly of the TRAF6-ECSIT complex for the juxtaposition of mitochondria and phagosomes. (**a**) Immunofluorescence microscopy of the co-localization (short thick arrows) of TRAF6 (red) and ECSIT (green) with bacteria in wild-type, cDKO and cDKO-Rac1^{G12V} BMDMs infected with *E. coli* (blue); outlined areas are enlarged 4× in insets in corners (connected by longer thinner arrows). Scale bars, 20 μm. (**b**) Immunoblot analysis of total lysates (bottom) and anti-Flag immunoprecipitates (top) of 293T cells expressing various combinations (above lanes) of Myc-tagged ECSIT, Flag-tagged TRAF6 and HA-tagged wild-type Rac1, Rac1^{G12V} or Rac1^{T17N}. (**c**) Immunoblot analysis of the association of active (GTP-bound) Rac2 with GST-PAK$^{70–106}$ in lysates of 293T cells expressing various combinations (above lanes) of Flag-tagged wild-type Rac2 or Rac2^{D57N} and Myc-tagged TRAF6, incubated with GST-PAK$^{70–106}$ (CoBlue, as in **Fig. 5d**). (**d**) Immunoassay (as in **b**) of 293T cells expressing various combinations (above lanes) of Flag-tagged wild-type Rac2 or Rac2^{D57N} and Myc-tagged TRAF6. (**e**) Immunoassay (as in **b**) of the competitive binding of ECIST and Rac2^{D57N} with TRAF6 293T cells expressing various combinations (above lanes) of HA-tagged ECSIT, Myc-tagged TRAF6 and Flag-tagged wild-type Rac2 or Rac2^{D57N}. (**f**) Flow cytometry of unstained wild-type cells expressing control vector (US ctrl) and of wild-type and cDKO BMDMs infected with adenovirus expressing control vector (Ad-CV), wild-type Rac2 (Ad-Rac2^{WT}) or Rac2^{D57N} (Ad-Rac2^{D57N}), then treated for 3 h with LPS and stained with MitoSOX or CellRox. (**g**,**h**) Immunofluorescence microscopy of the co-localization (arrows) of ECSIT (purple) and TRAF6 (red) with bacteria (blue) (**g**), and of mitochondrial networks (red; as in **Fig. 3a**) with bacteria (blue) (**h**), in wild-type BMDMs infected with adenovirus expressing wild-type Rac2 or Rac2^{D57N} and incubated with *E. coli*. Scale bars, 20 μm. Data are from one experiment representative of three independent experiments with similar results (**a**–**h**), with ~100 cells (**a**,**g**,**h**).

inactive Rac1^{T17N}, TRAF6 failed to ubiquitinate the inactive Rac2^{D57N} variant (**Supplementary Fig. 7e**). TRAF6 enhanced the GTP 'charging' of wild-type Rac2 but not that of inactive Rac2^{D57N} (**Fig. 7c**). Rac2^{D57N} bound to TRAF6 better than wild-type Rac2 did (**Fig. 7d**), and Rac2^{D57N} also efficiently dissociated TRAF6-ECSIT complexes (**Fig. 7e**). Furthermore, the induction of mROS and cellular ROS upon stimulation with LPS was blocked in wild-type BMDMs infected with adenovirus expressing Rac2^{D57N}, whereas cDKO BMDMs infected with adenovirus expressing wild-type Rac2 displayed normal production of mROS and cellular ROS upon stimulation with LPS (**Fig. 7f**). In addition, Rac2^{D57N} expressed by adenovirus also blocked formation of the ECSIT-TRAF6 complex (**Fig. 7g**) and mitochondrion-phagosome juxtaposition (**Fig. 7h**) during bacterial infection. These results indicated that GTP 'charging' and ubiquitination of Rac during bacterial infection of BMDMs was critical for the dissociation of Rac from the TRAF6 MATH domain to enable assembly of the TRAF6-ECSIT complex, and that this in turn mediated mitochondrion-phagosome juxtaposition and an increase in mROS production.

Rac1^{G12V} 'rescues' the Mst1- and Mst2-null phenotype

cDKO-Rac1^{G12V} BMDMs displayed normal F-actin organization, mitochondrion-phagosome association and mROS production upon stimulation with LPS or bacterial infection (**Fig. 3a**–**c**,**e**,**f** and **Supplementary Fig. 3a**). Furthermore, constitutively active Rac1^{G12V} fully 'rescued' the Mst1- and Mst2-deficient phenotype, as shown by the restoration of phagocyte bactericidal activity and normal resistance to bacteremia during CLP-induced bacterial sepsis (**Fig. 8**). These results demonstrated that the mediation of Rac activation by Mst1 and Mst2 was a critical event for phagocytes in the defense against infection. Together our findings have revealed

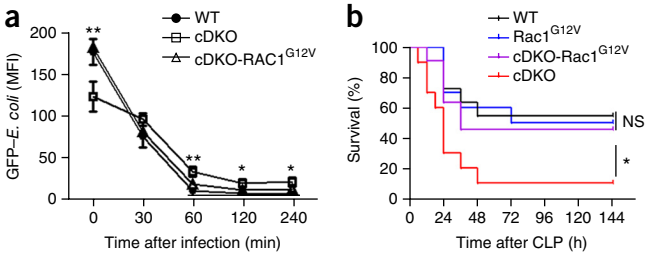

Figure 8 Rac1^{G12V} fully 'rescues' the Mst1- and Mst2-deficient phenotype. (**a**) Bacterial load in wild-type, cDKO and cDKO-Rac1^{G12V} BMDMs infected for 0–240 min with GFP–*E. coli* (presented as in **Fig. 2b**). $*P < 0.05$ and $**P < 0.01$, cDKO versus cDKO-Rac1^{G12V} (Student's *t*-test). (**b**) Mortality of wild-type mice ($n = 11$), Rac1^{G12V} mice ($n = 10$), cDKO-Rac1^{G12V} mice ($n = 11$) and cDKO mice ($n = 10$) subjected to sublethal CLP. $*P = 0.046$, cDKO versus cDKO-Rac1^{G12V} (Mantel–Cox test). Data are from one experiment representative of three independent experiments with similar results (mean ± s.d. of $n = 5$ in **a**).

TLR-Mst1-Mst2-PKC-Rac-TRAF6-ECSIT signaling in phagocytes as an important bactericidal mechanism (**Supplementary Fig. 8a**).

DISCUSSION

Large amounts of ROS are generated in phagocytes upon stimulation and phagocytosis, and this is necessary for the killing of ingested pathogens. How phagocytes generate these large amounts of ROS remains incompletely understood. Here we identified a previously unknown aspect of TLR signaling involved in host defense: the role of Mst1 and Mst2 in the activation of Rac and the recruitment of mitochondria to phagosomes for optimal ROS production. The stimulation of cell-surface TLRs activated Mst1 and Mst2 to phosphorylate and stimulate PKC-α, which in turn phosphorylated LyGDI and caused the release of inactive GDP-bound Rac. Once 'charged' with GTP, Rac underwent K63-linked ubiquitination by TRAF6, which augmented further 'charging' of Rac with GTP. The importance of the contribution of Mst1 and Mst2 to such 'charging' was shown by the ability of myeloid cell–specific expression of constitutively active Rac1^{G12V} to restore the defective mitochondrion-phagosome association and eliminate the enhanced susceptibility to bacterial infection of mice lacking myeloid cell expression of Mst1 and Mst2. Thus, Mst1 and Mst2 are critical components of signaling via TLR1, TLR2 and TLR4 that support host defense against invading pathogens.

Macrophages generate mROS through TLR signaling in response to bacteria, and they do so by coupling this signaling to mitochondrial complex I by promoting the association of TRAF6 with the mitochondrial complex I–assembly factor ECSIT[11]. Nevertheless, the mechanisms by which TLR signaling engages components from both mitochondria and phagosomes to form the active oxidase machinery for ROS production remain incompletely defined. Here we found that TRAF6 mediated the ubiquitination of Rac and maintained its active, GTP-bound state for full activation of the ROS-generating machinery during an antimicrobial response. The inactivating D57N substitution in human Rac2 (Rac2^{D57N}) results in a substantial reduction in the production of ROS by phagocytes and leads to severe bacterial infections, a phenotype similar to that of mice doubly deficient in Mst1 and Mst2 (refs. 8,9). We found that signaling via Mst1 and Mst2 controlled mitochondrial trafficking and the mitochondrion-phagosome association by stimulating activation of Rac. GTP-bound Rac, in addition to serving a key role in the activation of NADPH oxidase, mediated the actin reorganization required for the trafficking of mitochondria to phagosomes. Rac2^{D57N} bound to GDP but not to GTP, and Rac-GDP bound competitively to TRAF6 with ECSIT and thereby prevented formation of the TRAF6-ECSIT complex and the association of mitochondria with phagosomes. Thus, Rac is a key downstream regulator of mROS and phagosomal ROS, and the stimulation of Rac activation by Mst1 and Mst2 is critical for optimal ROS production during the phagocytosis of pathogens.

In summary, our work has demonstrated that kinases Mst1 and Mst2 are key regulators of microbe-elicited ROS production and that they act through a previously unrecognized signaling cascade: TLR-Mst1-Mst2-PKC-Rac-TRAF6-ECIST. The downstream effectors of the TLR-MyD88 complex for the activation of Mst1 and Mst2 remain to be identified. The kinase Mst4 has been shown to limit inflammatory responses through direct phosphorylation of TRAF6 (ref. 45). Future studies should determine whether Mst1 and Mst2 can also phosphorylate TRAF6 and, if so, whether this affects the TRAF6-mediated regulation of Rac activation. Studies have shown that the phosphorylation of transcription factors of the Foxo family by Mst1 protects against neuronal cell death induced by oxidative stress[46–48]. However, the Mst1-Foxo pathway in cells of the immune system still remains controversial[33,35,40]. Thus, additional studies are needed to identify in full the mechanisms through which TLR-Mst1-Mst2 signaling regulates microbe-elicited production of ROS during an antimicrobial response and thereby regulates killing of the pathogens and the self-antioxidant defense needed for cell survival. Such studies will provide molecular insight that will aid in the design of therapeutic agents for antimicrobial infection.

METHODS

Methods and any associated references are available in the online version of the paper.

Note: Any Supplementary Information and Source Data files are available in the online version of the paper.

ACKNOWLEDGMENTS

Supported by the National Basic Research Program (973) of China (2015CB910502 to L.C.), China's 1000 Young Talents Program (D.Z. and L.C.), the 111 Projects (B12001 and B06016), the Fundamental Research Funds for the Central Universities of China-Xiamen University (CXB2014004 to J.Z.; 20720140551 to L.C.; and 2013121034 and 20720140537 to D.Z.), the National Natural Science Foundation of China (31270918, 81222030 and J1310027 to D.Z.; 81372617, 81422018 and U1405225 to L.C.; 81472229 to L.H.; and 81302529 to X.L.), the Natural Science Foundation of Fujian (2013J06011 to D.Z. and 2014D007 to X.L.), the US National Institutes of Health (RO1 CA136567 for J.A.) and institutional funds from Massachusetts General Hospital (for J.A.). The funders had no role in study design, data collection and analysis, decision to publish, or preparation of the manuscript.

AUTHOR CONTRIBUTIONS

J.G., X.S., L.C. and D.Z. designed the research and helped with data analysis; J.G., X.S., P.W., S.Z., X.W., H.W., L.H., C.X., X.L., H.Z., Q.L., M.J., Q.C., J.Z., Y.L. and K.-Y.C. performed the experiments and helped with data analysis; S.S., H.-R.W., R.Z., R.L.J., S.-C.L., J.H. and J.A. contributed to discussions and provided critical reagents; and J.A., L.C. and D.Z. wrote the paper.

COMPETING FINANCIAL INTERESTS

The authors declare no competing financial interests.

1. West, A.P., Koblansky, A.A. & Ghosh, S. Recognition and signaling by toll-like receptors. *Annu. Rev. Cell Dev. Biol.* **22**, 409–437 (2006).
2. Beutler, B. *et al.* Genetic analysis of host resistance: Toll-like receptor signaling and immunity at large. *Annu. Rev. Immunol.* **24**, 353–389 (2006).

3. Lambeth, J.D. NOX enzymes and the biology of reactive oxygen. *Nat. Rev. Immunol.* **4**, 181–189 (2004).
4. Bedard, K. & Krause, K.H. The NOX family of ROS-generating NADPH oxidases: physiology and pathophysiology. *Physiol. Rev.* **87**, 245–313 (2007).
5. Bokoch, G.M. & Diebold, B.A. Current molecular models for NADPH oxidase regulation by Rac GTPase. *Blood* **100**, 2692–2696 (2002).
6. Mehta, D., Rahman, A. & Malik, A.B. Protein kinase C-α signals rho-guanine nucleotide dissociation inhibitor phosphorylation and rho activation and regulates the endothelial cell barrier function. *J. Biol. Chem.* **276**, 22614–22620 (2001).
7. DerMardirossian, C., Schnelzer, A. & Bokoch, G.M. Phosphorylation of RhoGDI by Pak1 mediates dissociation of Rac GTPase. *Mol. Cell* **15**, 117–127 (2004).
8. Ambruso, D.R. *et al.* Human neutrophil immunodeficiency syndrome is associated with an inhibitory Rac2 mutation. *Proc. Natl. Acad. Sci. USA* **97**, 4654–4659 (2000).
9. Williams, D.A. *et al.* Dominant negative mutation of the hematopoietic-specific Rho GTPase, Rac2, is associated with a human phagocyte immunodeficiency. *Blood* **96**, 1646–1654 (2000).
10. Gu, Y. *et al.* Biochemical and biological characterization of a human Rac2 GTPase mutant associated with phagocytic immunodeficiency. *J. Biol. Chem.* **276**, 15929–15938 (2001).
11. West, A.P. *et al.* TLR signalling augments macrophage bactericidal activity through mitochondrial ROS. *Nature* **472**, 476–480 (2011).
12. Sena, L.A. & Chandel, N.S. Physiological roles of mitochondrial reactive oxygen species. *Mol. Cell* **48**, 158–167 (2012).
13. Emre, Y. *et al.* Mitochondria contribute to LPS-induced MAPK activation via uncoupling protein UCP2 in macrophages. *Biochem. J.* **402**, 271–278 (2007).
14. Wu, W., Hsu, Y.M., Bi, L., Songyang, Z. & Lin, X. CARD9 facilitates microbe-elicited production of reactive oxygen species by regulating the LyGDI-Rac1 complex. *Nat. Immunol.* **10**, 1208–1214 (2009).
15. Arsenijevic, D. *et al.* Disruption of the uncoupling protein-2 gene in mice reveals a role in immunity and reactive oxygen species production. *Nat. Genet.* **26**, 435–439 (2000).
16. Bulua, A.C. *et al.* Mitochondrial reactive oxygen species promote production of proinflammatory cytokines and are elevated in TNFR1-associated periodic syndrome (TRAPS). *J. Exp. Med.* **208**, 519–533 (2011).
17. Creasy, C.L., Ambrose, D.M. & Chernoff, J. The Ste20-like protein kinase, Mst1, dimerizes and contains an inhibitory domain. *J. Biol. Chem.* **271**, 21049–21053 (1996).
18. Creasy, C.L. & Chernoff, J. Cloning and characterization of a human protein kinase with homology to Ste20. *J. Biol. Chem.* **270**, 21695–21700 (1995).
19. Rawat, S.J. & Chernoff, J. Regulation of mammalian Ste20 (Mst) kinases. *Trends Biochem. Sci.* **40**, 149–156 (2015).
20. Avruch, J. *et al.* Protein kinases of the Hippo pathway: regulation and substrates. *Semin. Cell Dev. Biol.* **23**, 770–784 (2012).
21. Zhou, D. *et al.* Mst1 and Mst2 maintain hepatocyte quiescence and suppress hepatocellular carcinoma development through inactivation of the Yap1 oncogene. *Cancer Cell* **16**, 425–438 (2009).
22. O'Neill, E., Rushworth, L., Baccarini, M. & Kolch, W. Role of the kinase MST2 in suppression of apoptosis by the proto-oncogene product Raf-1. *Science* **306**, 2267–2270 (2004).
23. Del Re, D.P. *et al.* Mst1 promotes cardiac myocyte apoptosis through phosphorylation and inhibition of Bcl-xL. *Mol. Cell* **54**, 639–650 (2014).
24. Maejima, Y. *et al.* Mst1 inhibits autophagy by promoting the interaction between Beclin1 and Bcl-2. *Nat. Med.* **19**, 1478–1488 (2013).
25. Pan, D. The hippo signaling pathway in development and cancer. *Dev. Cell* **19**, 491–505 (2010).
26. Harvey, K.F., Zhang, X. & Thomas, D.M. The Hippo pathway and human cancer. *Nat. Rev. Cancer* **13**, 246–257 (2013).
27. Yu, F.X. & Guan, K.L. The Hippo pathway: regulators and regulations. *Genes Dev.* **27**, 355–371 (2013).
28. Johnson, R. & Halder, G. The two faces of Hippo: targeting the Hippo pathway for regenerative medicine and cancer treatment. *Nat. Rev. Drug Discov.* **13**, 63–79 (2014).
29. Zeng, Q. & Hong, W. The emerging role of the hippo pathway in cell contact inhibition, organ size control, and cancer development in mammals. *Cancer Cell* **13**, 188–192 (2008).
30. Zhou, D. *et al.* Mst1 and Mst2 protein kinases restrain intestinal stem cell proliferation and colonic tumorigenesis by inhibition of Yes-associated protein (Yap) overabundance. *Proc. Natl. Acad. Sci. USA* **108**, E1312–E1320 (2011).
31. Abdollahpour, H. *et al.* The phenotype of human STK4 deficiency. *Blood* **119**, 3450–3457 (2012).
32. Nehme, N.T. *et al.* MST1 mutations in autosomal recessive primary immunodeficiency characterized by defective naive T-cell survival. *Blood* **119**, 3458–3468 (2012).
33. Du, X. *et al.* Mst1/Mst2 regulate development and function of regulatory T cells through modulation of Foxo1/Foxo3 stability in autoimmune disease. *J. Immunol.* **192**, 1525–1535 (2014).
34. Dong, Y. *et al.* A cell-intrinsic role for Mst1 in regulating thymocyte egress. *J. Immunol.* **183**, 3865–3872 (2009).
35. Ueda, Y. *et al.* Mst1 regulates integrin-dependent thymocyte trafficking and antigen recognition in the thymus. *Nat. Commun.* **3**, 1098 (2012).
36. Katagiri, K., Imamura, M. & Kinashi, T. Spatiotemporal regulation of the kinase Mst1 by binding protein RAPL is critical for lymphocyte polarity and adhesion. *Nat. Immunol.* **7**, 919–928 (2006).
37. Katagiri, K., Maeda, A., Shimonaka, M. & Kinashi, T. RAPL, a Rap1-binding molecule that mediates Rap1-induced adhesion through spatial regulation of LFA-1. *Nat. Immunol.* **4**, 741–748 (2003).
38. Katagiri, K. *et al.* Crucial functions of the Rap1 effector molecule RAPL in lymphocyte and dendritic cell trafficking. *Nat. Immunol.* **5**, 1045–1051 (2004).
39. Zhou, D. *et al.* The Nore1B/Mst1 complex restrains antigen receptor-induced proliferation of naive T cells. *Proc. Natl. Acad. Sci. USA* **105**, 20321–20326 (2008).
40. Mou, F. *et al.* The Mst1 and Mst2 kinases control activation of rho family GTPases and thymic egress of mature thymocytes. *J. Exp. Med.* **209**, 741–759 (2012).
41. Raab, M. *et al.* T cell receptor "inside-out" pathway via signaling module SKAP1-RapL regulates T cell motility and interactions in lymph nodes. *Immunity* **32**, 541–556 (2010).
42. Sasai, M. & Yamamoto, M. Pathogen recognition receptors: ligands and signaling pathways by Toll-like receptors. *Int. Rev. Immunol.* **32**, 116–133 (2013).
43. Kawai, T. & Akira, S. Toll-like receptors and their crosstalk with other innate receptors in infection and immunity. *Immunity* **34**, 637–650 (2011).
44. Jiang, X. & Chen, Z.J. The role of ubiquitylation in immune defence and pathogen evasion. *Nat. Rev. Immunol.* **12**, 35–48 (2012).
45. Jiao, S. *et al.* The kinase MST4 limits inflammatory responses through direct phosphorylation of the adaptor TRAF6. *Nat. Immunol.* **16**, 246–257 (2015).
46. Lehtinen, M.K. *et al.* A conserved MST-FOXO signaling pathway mediates oxidative-stress responses and extends life span. *Cell* **125**, 987–1001 (2006).
47. Yuan, Z. *et al.* Regulation of neuronal cell death by MST1-FOXO1 signaling. *J. Biol. Chem.* **284**, 11285–11292 (2009).
48. Xiao, L. *et al.* The c-Abl-MST1 signaling pathway mediates oxidative stress-induced neuronal cell death. *J. Neurosci.* **31**, 9611–9619 (2011).

ONLINE METHODS

Animals. The conditional knockout of *Mst1* and *Mst2* has been described[40]. Wild-type C57BL/6, *Vav*-Cre mice (008610), *Lyz2*-Cre mice (004781) and C57BL/6-Gt(ROSA)26Sor$^{tm9(Rac1^*,EGFP)Rsky}$/J mice (012361) were originally from the Jackson Laboratory. All mice were maintained under specific pathogen–free conditions at the Xiamen University Laboratory Animal Center. These mouse experiments were approved by the Institutional Animal Care and Use Committee and were in strict accordance with good animal practice as defined by the Xiamen University Laboratory Animal Center.

Chemicals and reagents. Pam_3CSK_4, LTA, CpG, poly(I:C) and R848 were from InvivoGen. LPS, rotenone, antimycin A, cytochalasin D, MG132 (C2211), GDP (G7127) and GTPγS (G8634) were from Sigma-Aldrich. NSC23766 (1177865-17-6) was from Millipore. The Mitochondrial Membrane Potential Assay Kit with JC-1 was from Beyotime Biotech. Oligo nucleotides were synthesized by Sangon Biotech (**Supplementary Table 1**). The Phos-tag TM Acrylamide AAL-107 was from the NARD Institute.

Flow cytometry assays. Single cells isolated from the bone marrow, spleen, lymph nodes or blood were stained for 20 min with the appropriate fluorescence-conjugated antibodies and washed, then were resuspended with flow cytometry staining buffer (1% BSA in PBS) containing DAPI (4′,6-diamidino-2-phenylindole; (Invitrogen). Stained cells were analyzed with a BD LSRFortessa flow cytometer (BD Biosciences). Flow cytometry data were plotted and quantified, through the use of median fluorescence intensity, with FlowJo software (TreeStar). Fluorescence-conjugated anti-CD3ε (145-2C11), anti-CD62L (MEL14), anti-CD11b (M1/70), anti-B220 (RA3-6B2), anti-CD44 (IM7), anti-F4/80 (BM8) and anti-Gr-1 (RB6-8C5) were from BioLegend.

Measurement of ROS and mROS. For flow cytometry–based measurements, cells (RAW246.7 cells, BMDMs or neutrophils) were plated in non–tissue-culture-treated dishes and then were treated with various TLR agonists or infected with bacteria. The concentrations of stimulants were as follows: 1 μg/ml LPS, 1 μg/ml Pam_3CSK_4, 2 μg/ml LTA, 10 μg/ml poly(I:C), 1 μM CpG, 1 μg/ml R848, 500 nM rotenone, 1mg/ml oligomycin or 5 μM antimycin A. The culture medium was removed and then the cells were washed with PBS and then incubated for 30 min at 37 C with MitoSOX (for measurement of mROS superoxide; Invitrogen) and/or CM-H2DCFDA or CellROX (for measurement of total cellular H_2O_2; Invitrogen) at a final concentration of 2.5 μM in serum-free DMEM (Invitrogen). The cells were washed with warmed PBS, removed from the plates by pipetting with cold PBS containing 1 mM EDTA, pelleted at 1,500 r.p.m. for 3 min, immediately re-suspended in cold PBS containing 1% FBS and analyzed by flow cytometry.

For luminol-based ROS measurements, a total of 1×10^5 BMDMs or neutrophils in DMEM were seeded in each well of a luminometer plate with 10% (vol/vol) FBS. Before the assay, the cells were washed once with warm Hank's balanced-salt solution (HBSS) without phenol red. Then, 200 μl HBSS containing 100 μM luminol and 5 units of horseradish peroxidase (Sigma) was added to each well. Cells were incubated for 10 min at 37 °C, followed by stimulation with *L. monocytogenes* (MOI, 10) or *E. coli* (MOI, 20). ROS production was monitored every minute for 2 h with a luminometer (MRX Revelation 96-well multiscanner; Dynex Technologies).

Cell culture. The 293T, HeLa and RAW264.7 cell lines (from the American Type Culture Collection) were tested for mycoplasma contamination and were found to be negative, then were cultured in DMEM supplemented with 10% FBS and 1× penicillin-streptomycin (Invitrogen).

For BMDMs, the femur and tibia were collected from mice of each genotype, and bone marrow cells were flushed with complete DMEM containing 50 mg/ml streptomycin and 10% FBS. Erythrocytes were removed via treatment with red blood cell lysis buffer, and the cell suspensions were filtered through a 40-μm cell strainer for the removal of any cell clumps. The single-cell suspensions were then cultured for 1 h at 37 °C, and non-adherent cells were collected and re-plated in complete DMEM with 25% medium conditioned by L929 mouse fibroblasts. For full differentiation of BMDMs, the cells were cultured for an additional 8 d with replacement of the medium every 2 d. All cells were $CD11b^+F4/80^+$ when analyzed by flow cytometry.

For neutrophils, single-cell suspensions prepared from mouse bone marrow were subjected to Percoll gradient separation (81–62.5%) (GE Healthcare Life Sciences) by centrifugation at 1,600 r.p.m. for 30 min at room temperature. Neutrophils were collected from the interphase, then were washed twice, re-suspended in HBSS and used for further analysis. Cell purity was more than 90%, as shown by staining as $CD11b^+Gr1^+$ and analysis by flow cytometry.

Cytokine measurement. Cell supernatants or serum were collected at the appropriate time points after stimulation with LPS or after induction of CLP. The concentrations of mouse IL-6, TNF or IL-1β were measured with ELISA kits (BioLegend) or CBA kits (BD Bioscience) according to the manufacturers' instructions.

CLP. Mice were anesthetized, and an abdominal incision was made for identification of the cecum. The distal one third of the cecum was ligated with silk suture and was punctured once with a 21-gauge needle. A small amount of cecal content was extruded through the perforation. The peritoneum and skin was closed with a continuous suture after the cecum was returned to the abdomen. 1 ml saline was injected intraperitoneally for resuscitation. For sham-treated mice, all of the same steps were performed, except for ligation and puncture of the cecum.

Measurement of bacterial loads in tissues. Bacteria were counted in peritoneal fluid, liver, lung, kidney and spleen obtained aseptically. At 24 h after CLP or sham surgery, for analysis of peritoneal fluid, mice were killed and the skin of abdomen was cut open at the midline without injury to the muscle. Peritoneal fluid sample was serially diluted in PBS and was cultured on tryptose soy agar–blood agar plates. Colony-forming units (CFUs) were counted after 18–24 h of incubation at 37 °C, and the results are presented as $\log_{10}$ of the number of CFU per ml peritoneal fluid. Similar procedures were used for homogenates of liver, lung, kidney and spleen obtained 24 h after sham surgery or CLP. Values for CFU are presented as colony counts per gram of tissue.

Construction of GFP-expressing *E. coli*. The constitutive prokaryotic promoter BBa_J23100 was inserted upstream of the GFP generator BBa_E0840 in the vector pSB1A2. The product was transformed into DH5α-competent cells for acquisition of an *E. coli* strain stably expressing GFP (GFP–*E. coli*). The GFP generator BBa_E0840 was a gift from the iGEM team from the Ocean University of China. The sequence of the promoter BBa_J23100 was obtained from the online Registry of Standard Biological Parts.

Phagocytosis and bacteria-killing assay. For flow cytometry–based measurement of phagocytosis, a total of 1×10^6 wild-type and cDKO BMDMs or neutrophils in PBS were cooled down to 4 °C for 30 min. Then, the cells were left uninfected or were infected for 20 min at 37 °C or 4 °C with heat-killed, FITC-labeled and fresh mouse serum–opsonized *L. monocytogenes* (MOI, 10) or *E. coli* (MOI, 20), after which they were washed extensively with cold PBS twice and fixed with 4% paraformaldehyde. The fluorescence of extracellular particles was quenched by replacement of the medium with 0.2% Trypan blue in PBS, pH 5.5, shortly before the actual measurement by flow cytometry.

For measurement of phagocytosis and killing via analysis of immunofluorescence, a total of 2×10^5 BMDMs were grown on glass cover slips in 35-mm dishes. Cells were infected for 1 h with GFP–*E. coli* (MOI, 20), followed by several washes with PBS. Infected cells were further cultured in medium containing 10 μg/ml gentamicin. At the appropriate time points, the cells were washed in PBS and then fixed for 10 min at room temperature in 4% (vol/vol) paraformaldehyde. Slides were mounted with the mounting medium Vectashield (H1200; Vector Laboratories) containing DAPI and were imaged with a confocal microscope (Zeiss LSM 780; Zeiss). The mean pixel intensity of GFP was measured with Zeiss ZEN lite 2012 software. The ratio of the total area of GFP dots to overall cell number is plotted.

For the *in vitro* bacteria-killing assay, fresh overnight cultures of *E. coli* and *L. monocytogenes* were suspended in PBS and were opsonized with fresh

doi:10.1038/ni.3268

mouse serum. The BMDMs or neutrophils were incubated for the appropriate time at 37 °C, with intermittent shaking, with *E. coli* (MOI, 20) or *L. monocytogenes* (MOI, 10). After each time point, cells were lysed by the addition of distilled H_2O, and diluted aliquots were spread on LB agar plates (*E. coli*) or brain-heart–infusion agar plates (*L. monocytogenes*). CFU was assessed after incubation of the plates overnight at 37 °C.

Mitochondrial membrane potential assay. The mitochondrial membrane potential was measured with a dual-emission potential-sensitive probe (JC-1 dye) according to the manufacturer's instructions (Beyotime Biotech). Wild-type and cDKO BMDMs in a six-well plate were incubated for 20 min at 37 °C (in an incubator at 5% CO_2) with 1 ml of mitochondrial staining solution containing 1 ml culture medium and 2.5 μg/ml of JC-1 dye. The cells were then washed twice with warm PBS. Finally, images were viewed and scanned with a confocal microscope (Zeiss LSM 780) at 490-nm excitation and 530-nm emission for green and at 540-nm excitation and 590-nm emission for red.

SDS-PAGE, Phos-tag SDS-PAGE and immunoblot analysis. Gels for SDS-PAGE or Phos-tag SDS-PAGE were prepared according to the manufacturer's instructions (NARD Institute). Proteins were separated by SDS-PAGE or Phos-tag SDS-PAGE, were transferred onto a PVDF membrane and then were identified by immunoblot analysis with the appropriate primary antibodies at a dilution of 1:1,000 (or as otherwise stated below). Anti-HA (3724), antibody to phosphorylated p38 (9211), antibody to phosphorylated Jnk (9251), antibody to phosphorylated Erk (9101), anti-GAPDH (2118), anti-IκBa (4814), antibody to phosphorylated MARCKS (2741), anti-HSP60 (4870), anti-COX IV (4850), anti-CYCS (4280), anti-PHB1 (2426), anti–pyruvate dehydrogenase (3205), anti-SDHA (5839), anti-SOD1 (4266), anti-VDAC (4661), anti-NRF1 (12381), antibody to K63-linked polyubiquitin (5621), anti-ubiquitin (3936), anti-PKC-α (2056), anti-PKC-δ (9616) and anti-PKC-ζ (9372) were from Cell Signaling Technology. Anti-LyGDI (16122-1-AP), anti-TRAF6 (12809-1-AP), anti-HSP60 (66041-1-Ig), anti-MTERF (16957-1-AP) and anti-TFAM (19998-1-AP) were from Proteintech Group. Anti-ACO2 (AB61224a) was from Sangon Biotech. Anti-TRAF6 (ab181622), anti-Rac1 (ab33186) and anti-PGC-1a (ab106814) were from Abcam. Anti-Rac1 (sc-217), anti-HA (sc-7392), anti-Myd88 (sc-11356) and anti-ECSIT (sc-79473) were from Santa Cruz. Anti-β-actin (1:5,000 dilution; a2066) and anti-Flag (1:5,000 dilution; F1804) were from Sigma. Anti-Mst1, anti-Mst2 and antibody to Mob1 phosphorylated at Thr35 have been described[49]. Horseradish peroxidase–conjugated antibody to rabbit IgG (7074) or to mouse IgG (7076) (1:3,000 dilution for each) were from Jackson ImmunoResearch Laboratories. The protein bands were visualized woth a SuperSignal West Pico Kit according to the manufacturer's instructions (Thermo Fisher Scientific Pierce).

***In vitro* kinase assay.** Mst2 kinase was expressed as a Flag-tagged protein in HEK293T cells. The Mst2 kinase assay was performed by incubation of Flag-tagged Mst2, immunoprecipitated with anti-Flag, together with recombinant GST–PKC-α amino terminus (amino acids 1–338) or GST–PKC-α amino terminus with the S226A substitution (each purified in bacteria) in a kinase assay buffer containing 2 mM dithiothreitol, 10 mM $MgCl_2$, 50 μM ATP, 40 mM HEPES (pH 7.4) and 1 mM EDTA. The reactions were incubated for 30 min at 30 °C before SDS-PAGE and immunoblot analysis.

Staining with hematoxylin and eosin. The tissue specimens were fixed for 24 h in 10% neutral-buffered formalin and then were dehydrated in increasing concentrations of isopropyl alcohol, followed by clearing of alcohol by xylene. The specimens were subsequently embedded in paraffin wax in cassettes for facilitation of tissue sectioning. Standard staining with hematoxylin and eosin was performed on sections 5 μm in thickness from each specimen block.

Assay of the GTP 'charging' of endogenous and recombinant Rac1. 293T cells seeded in a 60-mm dish at 85% confluence were transfected with the appropriate constructs. At 48 hours after transfection, the cells were harvested and then were lysed in binding buffer (50 mM Tris-HCl, pH 7.5, 150 mM NaCl, 1% Triton X-100, 10 mg/ml leupeptin, 10 mM NaF, 2 mM Na_3VO_4 and 1 mM PMSF). For BMDMs, cells seeded in a 60-mm dish at 80% confluence were harvested in binding buffer. *E. coli*–purified GST-PAK1-CRIB (20 μg) preloaded onto GSH Sepharose was incubated for 2 h at 4 °C with the pre-cleared cell lysates. After three washes with binding buffer, the amount of Rac-GTP bound to the beads was determined by SDS-PAGE, followed by immunoblot analysis of Flag or Rac1.

***In vivo* and *in vitro* ubiquitination assay.** For the *in vivo* ubiquitination assay, 293T cells were transfected for 36 h with the appropriate plasmids and were lysed in ice-cold lysis buffer ('TNTE 0.5%': 50 mM Tris-HCl, pH 7.5, 150 mM NaCl, 1 mM EDTA and 0.5% Triton X-100, containing 10 mM NaF, 2 mM Na_3VO_4, 10 mg/ml leupeptin and 1 mM PMSF). The cell lysates were then subjected to immunoprecipitation with anti-Flag, then were eluted by being boiled for 10 min in 1% SDS, were diluted 10 times in lysis buffer 'TNTE 0.5%' and then were re-immunoprecipitated with anti-Flag (two immunoprecipitations). The ubiquitin-conjugated proteins were detected by immunoblot analysis with the appropriate antibodies. For *in vitro* ubiquitination reactions, GST-Rac1-Flag and GST-TRAF6 proteins expressed by bacteria were purified with glutathione sepharose beads in 'TNTE 0.5%' buffer. Ubiquitination reactions were carried out with 0.3 mg Rac1, 0.35 mg rabbit E1 ubiquitin–activating enzyme (Boston Biochem), 0.4 mg UBE2N-UEV1A recombinant E2 complex (Boston Biochem), and 10 mg ubiquitin (Boston Biochem) in 20 μl ubiquitin-conjugation reaction buffer (50 mM Tris-HCl, pH 7.5, 10 mM $MgCl_2$ and 0.05 mM dithiothreitol, supplemented with 5 mM ATP). Rac1 was loaded with GTPγS or GDP or was left in its Mg^{2+}-free GDP-GTP 'empty' form, as described[50].

shRNA and lentiviral infection. Lentivirus was produced by co-transfection of 293T cells with shRNA in the vector pll3.7, VSV-G and Δ8.9 plasmids, through the use of Lipofectamine 2000 (Invitrogen). The shRNA was as follows: TRAF6-specific shRNA-1 (5′-GGTTGCCGAAATGGAAGCA-3′), TRAF6-specific shRNA-2 (5′-GAGAACAGATGCCTAATCA-3′), TRAF6-specific shRNA-3 (5′-CAGAACTGCTTGCCTTTCA-3′) and control shRNA (5′-GCAAGCTGACCCTGAAGTTC-3′). The most efficient shRNA was TRAF6-specific shRNA-1. Viral supernatants were harvested at 48–72 h after transfection, then were passed through a 0.45-μm filter, diluted 2:3 with fresh medium containing 8 μg/ml polybrene and used to infect the target cells at 80% confluence. Protein expression was visualized by immunoblot analysis.

Latex bead phagocytosis assay. Yellow-green 3-μm Fluoresbrite carboxy latex microparticles (Polysciences) were left untreated or were coated overnight at 4 °C with 30 μg/ml LPS or Pam_3CSK_4 in PBS. The beads were washed ten times in large volumes of PBS containing 1% FBS for removal of unbound TLR agonists. BMDMs were cultured on coverslips in six-well dishes and were incubated for 10 min on ice. Microparticles were added at a concentration of approximately four to eight beads per cell and were allowed to settle on the cells for an additional 10 min on ice. Warm medium was added to the cells, and the plates were warmed to 37 °C for the appropriate time to allow bead phagocytosis. Cells were then fixed for 20 min at room temperature with 3.7% paraformaldehyde, were permeabilized with 0.1% Triton X-100 and were stained with anti-Hsp60 (1:100 dilution; 66041-1; Proteintech) and Alexa Fluor 555–conjugated anti–mouse IgG (1:100 dilution; A31570; Invitrogen) for confocal microscopy (Zeiss LSM 780).

CFSE labeling. BMDMs were labeled for 8 min at 37 °C with 2.5 μM CFSE (carboxyfluorescein diacetate succinimidyl ester) according to manufacturer's instructions (Invitrogen), then were washed three times in complete DMEM, digested with trypsin and mixed with unlabeled cells.

Confocal fluorescence microscopy. For fluorescence analysis of F-actin, cells on coverslips were fixed for 10 min with 3.7% paraformaldehyde and were washed three times for 5 min each with 0.1% Triton X-100 in PBS. F-actin in cells was stained with Actin-Tracker Green (FITC-labeled phalloidin; Beyotime) in a solution containing 0.1% Triton X-100 and 5% BSA in PBS. After incubation for 50 min at room temperature, the cells were washed extensively, then were mounted and imaged uwith a fluorescence microscope (Zeiss LSM 780).

For fluorescence analysis of other molecules, BMDMs seeded on glass coverslips in six-well dishes were incubated for 30 min with GFP–*E. coli* or FITC-labeled heat-inactivated *L. monocytogenes*. HeLa cells seeded on

coverslips in six-well dish with 30% confluence were transfected with the appropriate constructs and were cultured for another 24 h. The cells were washed three times with PBS and were fixed for 15 min at room temperature with 4% (vol/vol) paraformaldehyde, after which additional immunofluorescence staining was applied. For staining with anti-Hsp60 (1:100 dilution; 66041-1; Proteintech), Rac1 (1:100 dilution; ab33186; Abcam), anti-TRAF6 (1:100 dilution; 12809; Proteintech), anti-ECSIT (1:100 dilution; sc-79473; Santa Cruz), anti–OctA (Flag) tag (1:250 dilution; sc-807; Santa Cruz), anti–Myc tag (1:250 dilution; sc-40; Santa Cruz) or anti–HA tag (1:250 dilution; sc-7392; Santa Cruz), fixed cells were rinsed with PBS and then were incubated for 10 min on ice with 0.2% Triton X-100 and 0.2% BSA in PBS. Following permeabilization, nonspecific binding in the cells was blocked by incubation for 30 min at room temperature with 0.02% Triton X-100 and 5% BSA in PBS and cells were incubated for 1 h with specific primary antibodies (identified above). After three washes with PBS, the cells were incubated for another 1 h with secondary antibodies (Alexa Fluor 488–conjugated anti–mouse IgG (A21202), Alexa Fluor 488–conjugated anti–rabbit IgG (A21206), Alexa Fluor 555–conjugated anti–mouse IgG (A31570), Alexa Fluor 555–conjugated anti–rabbit IgG (A31572) or Alexa Fluor 488–conjugated donkey anti–goat IgG (A11055) (all from Invitrogen). Subsequently, the cells were washed three times with PBS and were mounted with Vectashield mounting medium containing DAPI. All images were collected with a confocal microscope (Zeiss LSM 780).

Statistical analysis. All statistical analyses were performed with Prism5 software (GraphPad Software). Student's *t*-test was used for comparisons between two groups. Survival data were analyzed by the Kaplan-Meier statistical method. A *P* value of less than 0.05 was considered statistically significant.

49. Praskova, M., Xia, F. & Avruch, J. MOBKL1A/MOBKL1B phosphorylation by MST1 and MST2 inhibits cell proliferation. *Curr. Biol.* **18**, 311–321 (2008).
50. Torrino, S. *et al.* The E3 ubiquitin-ligase HACE1 catalyzes the ubiquitylation of active Rac1. *Dev. Cell* **21**, 959–965 (2011).

doi:10.1038/ni.3268